Environmental Science

AIMS Environmental Science, 13(2): 362–394.
DOI: 10.3934/environsci.2026015
Received: 26 December 2025
Revised: 18 March 2025
Accepted: 31 March 2025
Published: 29 April 2026

https://www.aimspress.com/journal/environmental

Research article

Innovative biochar adsorbent from *Parthenium hysterophorus* for carcinogenic lead removal: A step toward cleaner water and sustainable materials

Kamran Younas[1,*], Asma Jamil[1], Mahtab Ahmad[2], Nazish Iftikhar[3], Qaisar Mahmood[4,5], Yung-Tse Hung[6,*]

[1] Department of Earth and Environmental Sciences, Bahria School of Engineering and Applied Sciences (BSEAS), Bahria University, H-11 Campus, Islamabad, Pakistan
[2] Department of Environmental Sciences, Faculty of Biological Sciences, Quaid-i-Azam University, Islamabad 45320, Pakistan
[3] Institute of Environmental Science and Engineering, School of Civil and Environmental Engineering, National University of Science and Technology (NUST), Islamabad 44000, Pakistan
[4] Department of Biology, College of Science, University of Bahrain, Sakhir 32038, Bahrain
[5] Department of Environmental Sciences, COMSATS University Islamabad, Abbottabad Campus, Abbottabad, Pakistan
[6] Department of Environmental Engineering, Cleveland State University, Cleveland, OH, USA

* **Correspondance:** Email: kamranchemist36@gmail.com; y.hung@csuohio.edu.

Abstract: The study involved pyrolyzing biomass from *Parthenium hysterophorus* at temperatures of 300, 500, and 700°C to generate charcoal adsorbents (PTC 300, PTC 500, and PTC 700) at reduced prices. Subsequently, the PTCs were evaluated for their efficacy in eliminating Pb (II) from industrial effluent. Through the manipulation of operational parameters and the analysis of mathematical models, PTC 500 exhibited the highest adsorption capacity among the synthesized adsorbents, achieving 20.40 mg Pb (II)/g. The major mechanisms for Pb (II) adsorption onto biochar derived from *P. hysterophorus* are ion exchange with inherent mineral cations and surface complexation with oxygenated functional groups (-COOH, -OH). The enhanced immobilization efficacy is due to electrostatic attraction and lead precipitation within the pores of biochar. The pseudo-first order and Langmuir models provided the most precise characterization of Pb (II) adsorption onto PTCs in the batch adsorption study. An increased Pb (II) concentration, reduced flow velocity, and elevated bed

height collectively enhanced Pb (II) sorption in the fixed bed column. The Clark model most accurately represented the adsorption process and aligned with the experimental data in comparison to the other column models (Thomas, Yoon-Nelson, Clark, and Bohart-Adams models). The supplemental experimental results were consistent with the breakthrough curves. The maximum adsorption capacity achieved using the column approach was 8.16 mg/g. In contrast to rival adsorbents, PTCs exhibited significant reusability potential and enhanced adsorption efficiency.

Keywords: invasive biomass valorization; environmental sustainability; circular economy; lead contamination; water purification

1. Introduction

Heavy metals, such as lead (Pb), are among the hazardous pollutants in industrial effluent, posing significant risks to the environment and public health. Lead accumulates in cells and is classified as a carcinogenic and non-biodegradable pollutant. This may result in enduring health consequences such as cancer, renal impairment, and neurological disorders [1]. Lead contamination of rivers due to mining, battery production, electroplating, and pigment manufacturing has raised significant alarm, especially in developing countries with sometimes insufficient wastewater treatment systems. Consequently, the elimination of lead from industrial effluent is a significant environmental and public health concern, especially in poorer countries where sewage treatment facilities are often inadequate [2]. In wastewater treatment, fundamental approaches for heavy metal removal, such as ion exchange, chemical precipitation, coagulation-flocculation, and membrane filtration, have been widely employed [3,4]. Nevertheless, these methods sometimes produce hazardous secondary waste requiring further treatment, substantial operational costs, and intricate logistics. Consequently, there has been a surge in demand for economical, sustainable, and environmentally friendly alternatives. Adsorption-based treatment approaches have garnered significant interest due to their user-friendliness, efficacy, and ability to handle trace contaminants. Biochar, a carbon-dense material generated from the pyrolysis of biomass in low-oxygen conditions, has demonstrated potential as an adsorbent for the extraction of heavy metals. High porosity, extensive surface area, numerous surface functional groups, and robust stability are significant physicochemical properties of biochar that enhance its capacity to bind heavy metals [5].

The emphasis has shifted to producing biochar from low-cost, locally available materials such as invasive plants, forestry byproducts, and agricultural waste. The invasive alien plant *P. hysterophorus* has attracted attention due to its rapid growth, wide distribution, and harmful impacts on biodiversity and agriculture [6]. Despite being a significant ecological and economic threat in numerous regions, converting this weed into biochar yields two beneficial environmental outcomes: It mitigates the proliferation of the invasive species and provides a sustainable adsorbent for wastewater treatment. According to studies [7–9] , biochar made from parthenium and other lignocellulosic wastes has a great deal of promise for eliminating hazardous heavy metals, especially lead, from tainted water by means of surface complexation, ion exchange, and magnetism. Consequently, using biochar derived from parthenium weed to extract toxic lead from industrial effluent represents an innovative and sustainable approach that integrates environmental conservation with waste valorization [10]. Biochar is esteemed for its environmental benefits; yet, there are risks linked to its improper production or utilization. Biochar may contain heavy metals, ash, or residual polycyclic aromatic hydrocarbons (PAHs),

contingent upon the feedstock and pyrolysis conditions. If biochar is not properly stabilized, recycled, or disposed of after absorbing heavy metals such as Pb (II), the residual biochar is classified as secondary hazardous waste [11].

Research has emphasized the significance of underutilized biomass sources, such as invasive plant species, forestry outputs, and agricultural wastes, for biochar production. Parthenium hysterophorus is an exceptionally invasive species of international significance. It is a toxic weed that presents health hazards to humans and livestock, results in considerable agricultural losses, and diminishes biodiversity. It is an ideal candidate for conversion into charcoal owing to its rapid growth and low economic value. Producing biochar from parthenium mitigates its environmental impact while generating a sustainable adsorbent material. Studies have demonstrated that various forms of biochar can sequester toxic elements such as lead via surface complexation, ion exchange, and electrostatic attraction [12].

Adsorption may be conducted continuously or in discrete batches. Although continuous research data on adsorption is essential for the practical application of wastewater treatment, batch adsorption trials are vital for acquiring the necessary knowledge regarding the removal of specific pollutants. Continuous adsorption is often conducted in a fixed-bed column, where wastewater interacts with an adsorbent medium. In continuous adsorption, wastewater consistently flows into and out of the column, while the concentrations of the adsorbent and solution ions within the column vary, hence sustaining dynamic equilibrium. The consequences of continuous adsorption are assessed through column absorption capacity, breakthrough curve profile, and efficacy in contaminant removal. Operating variables such as bed depth, bed width, flow rate, and beginning pollutant concentration influence these characteristics [13]. The application of biochar derived from Parthenium weeds for lead removal in industrial wastewater has not garnered as much focus as biochar produced from forestry and agricultural residues. Bridging this gap is particularly crucial in regions with significant Parthenium infestations and industrial effluents. In this study, we aim to evaluate the adsorption efficacy of biochar derived from Parthenium weed for the removal of hazardous lead from industrial effluent. This study elucidates adsorption capacities and mechanisms, providing an innovative strategy for managing invasive weed species and promoting the development of eco-friendly, cost-effective, and sustainable wastewater remediation solutions.

This study is notable, as we utilize a poisonous plant to produce biochar, demonstrating competitive adsorption effectiveness relative to alternative adsorbents, and employ a dual experimental methodology to enhance understanding of scalability. PTCs appear to be a viable eco-friendly solution for industrial wastewater treatment, fostering the circular economy and environmental restoration, owing to their reusability and cost-effectiveness. We enhance biochar-based adsorption by tackling practical issues in continuous-flow systems through the integration of waste valorization and efficient Pb (II) removal. Biochar formed from *Parthenium hysterophorus* exhibits a complex adsorption process, unlike biochars produced from conventional agricultural waste, where adsorption effectiveness is primarily governed by surface area and nonspecific physical adsorption. Due to its mineral-rich biomass content, Parthenium biochar possesses several exchangeable cations that facilitate the removal of Pb (II) through ion exchange, and it forms strong complexes with oxygen-containing functional groups on its surface [14]. Furthermore, the hierarchically organized pores facilitate effective pore-filling processes and enhance mass transfer [15]. A notable advancement of this study is the incorporation of chemically active sites within an accessible porous structure in Parthenium hysterophorus biochar, distinguishing it from other biochars utilized in agriculture [16].

This paper offers an extensive analysis of batch and fixed-bed column systems, linking the technical elements of laboratory-scale investigations with real-world applications in the field. To attain

a more profound understanding of the adsorption capacity and kinetics, multiple isotherm models are analyzed and correlated with the experimental results. The reutilization capacity of these agro-weed adsorbents is examined for each PTC. The reusability and cost-effectiveness of PTCs highlight their potential as a sustainable solution for industrial wastewater treatment, aligning with the ideals of the circular economy and environmental restoration. We tackle practical issues in continuous-flow systems by combining waste valorization with efficient Pb (II) removal, thus progressing the domain of biochar-based adsorption.

2. Materials and methods

2.1. Chemicals and composition of Pb (II) solution

A 1000 mg/L Pb (II) stock solution was prepared using lead nitrate [Pb $(NO_3)_2$] and subsequently diluted with deionized water for batch adsorption investigations. The solution was formulated utilizing deionized water. We also employed other chemicals supplied by Sigma Aldrich, such as potassium hydroxide (KOH), sodium hydroxide (NaOH), sulfuric acid (H_2SO_4), nitric acid (HNO_3), and hydrochloric acid (HCl). Each chemical exhibited a purity of 99%. Column and batch studies were performed utilizing genuine industrial effluent, with samples obtained from the Hattar Industrial region (33.8507 °N, 72.85005 °E) battery manufacturing facility that produces lead batteries. The untreated samples were collected and stored at 4 ℃ in a refrigerator. Conventional methods were utilized for the characterization of the substance [17].

2.2. Collection of Parthenium and production of biochar

Approximately 20 kg of fresh parthenium weed (*P. hysterophorus*) was collected from several sites in the Rawalpindi district of Pakistan (33.232578N, 73.390846E). The biomass was desiccated under sunlight following purification with distilled water to eliminate residual dust. To diminish the moisture content to below 10%, it was further mechanically pulverized into smaller fragments of around 3 cm and desiccated in an oven maintained at 105 ℃ [18]. Subsequently, the feedstock was densely packed within ceramic crucibles and sealed with lids. Subsequently, the crucibles were placed in a Vulcan D-550 muffle furnace in the United States for pyrolysis. The feedstock underwent pyrolysis for 120 minutes at a steady rate of 5 ℃ per minute over three temperatures: 300, 500, and 700 ℃. Subsequent to pyrolysis, the resultant biochars (identified as PTC 300, PTC 500, and PTC 700, with PTC denoting the biochar and the numeral indicating the pyrolysis temperature) were permitted to cool to ambient temperature within a desiccator prior to being sieved through a 1.5 mm screen to ensure uniform particle size. The biochar yield was determined using the equation provided below [19].

2.3. Batch adsorption study

Experiments were performed on an orbital shaker (KJ-201, BD, China) at 150 rpm. Due to its remarkable purity, consistency, and minimal chemical interaction, it guarantees reproducibility and reduced Pb (II) retention [20]. The samples were initially filtered with Whatman #42 filter paper and subsequently analyzed using an atomic absorption spectrophotometer (AAS) (BK-AA320N Shimadzu, Japan) to determine the residual concentration of Pb (II) [21]. Control samples, which lacked PTCs, were also analyzed for each group. To validate the results, three replicates of each adsorption test were

performed. The quantity of Pb (II) extracted and assimilated was determined using Eqs (1) and (2), respectively:

$$\text{Removal}\ (\%) = \frac{C_i - C_e}{C_i} \times 100 \tag{1}$$

$$\text{Adsorption capacity}\ (\text{mg/g}) = \left[\frac{C_i - C_e}{W}\right] \times V \tag{2}$$

where 'C_i' is the initial Pb (II) concentration (mg/L), 'C_e' is the equilibrium Pb (II) concentration (mg/L), 'W' is the weight of PTC (g), and 'V' is the volume of solution (L).

Through a systematic set of experiments, the working conditions were optimized to attain the highest lead removal efficiency. Initially, the following parameters were held constant during the investigation: A total of 10 mg/L Pb (II) content, 1.5 g/L PTC dosage, wastewater temperature of 25 ± 2 ℃, and a 24-hour adsorption duration. Following the modification of the initial Pb (II) concentration from 0.5 to 15 mg/L, while keeping all other parameters constant, the PTC adsorbent dosage was optimized within the range of 0.2 to 3.5 g/L and a pH spectrum of 2 to 14. An assessment and enhancement of the interaction duration ranging from 10 to 1440 minutes was performed [22].

2.4. Adsorption isotherm and kinetic models

Four distinct isotherm models (Langmuir, Temkin, Freundlich, and Dubinin-Radushkevich) were utilized to analyze Pb (II) adsorption data for certain PTCs. The non-linear forms of the models were employed as delineated in Eqs (3)–(6), and the bonding energy was computed using Eq (7).

$$\text{Langmuir: } Q_e = \frac{Q_{max} \times K_L \times C_e}{1 + K_L \times C_e} \tag{3}$$

$$\text{Freundlich: } Q_e = K_F C_e^{1/n} \tag{4}$$

$$\text{Temkin: } Q_e = \frac{RT}{B} \text{Ln}(AC_e) \tag{5}$$

$$\text{Dubunin-Radushkevich: } Q_e = Q_D \exp\left[-B_D \left\{RT \ln\left(1 + \frac{1}{C_e}\right)\right\}^2\right] \tag{6}$$

$$E = \frac{1}{(2B_D)^{0.5}} \tag{7}$$

where 'n' is the adsorption strength constant, 'R' is gas constant (8.314 J/mol/K), 'T' is absolute temperature (K), 'B' is heat of adsorption (kJ/mol), 'A' is binding constant (L/mg), 'Q_D' is the Dubinin's adsorption capacity (mg/g), 'B_D' is the energy constant (mol^2/kJ^2), 'E' is the energy of bonding (kJ/mol), and 'Q_{max}' is Langmuir's maximum adsorption capacity (mg/g).

The following three kinetic models, Eqs (8)–(10), were used in their non-linear geometries to help explain the Pb (II) sorption onto PTCs [23]:

$$\text{Pseudo first order: } q_t = q_e(1 - e^{-k_1' t}) \tag{8}$$

$$\text{Pseudo second order: } q_t = \frac{k_2' q_e^2 t}{1 + k_2' q_e t} \tag{9}$$

$$\text{Elovich: } Q_t = \frac{1}{\beta} \text{Ln}(\alpha\beta t + 1) \tag{10}$$

where 't' is the contact period (min), 'α' is the rate of adsorption (mg/g-min), 'β' is sorption constant (g/mg), 'q_e' is the equilibrium Pb (II) concentration (mg/g), and 'k_1' (1/min) and 'k_2' (g/mg-min) are the rate constants for pseudo first order and pseudo second order, respectively.

2.5. Reuse of adsorbent

A desorption experiment was done on PTC 500 using five distinct 0.1N regeneration agents (CH_3COOH, H_2SO_4, HCl, NaOH, NaCl) to evaluate its potential for reuse after Pb (II) adsorption. The PTC 500, including Pb (II), was agitated at 150 rpm for one hour, mixed with the suitable desorbing agent, and the aqueous concentration of Pb (II) was measured by AAS. Two-step screening approaches were employed as per the methodology delineated to efficiently recover PTC 500 post-washing [18]. The suspension was initially filtered using Whatman # 42 filter paper. This initial filtration stage reduced the likelihood of the finer membrane becoming obstructed by eliminating coarse particles. The filtrate was subjected to vacuum filtration over a 0.22 μm nylon-cellulose membrane following partial clarification to guarantee the total retention of submicron PTC 500 particles, resulting in a clear solution appropriate for AAS [24]. These measures were integrated to optimize throughput, retention effectiveness, and analytical precision. The resultant aqueous concentration of Pb (II) was quantified utilizing Eq (11).

$$\text{Desorption } \% = \left.\text{Total of Pb (II) desorbed (mg/g)}\right/\text{Total of Pb(II) adsorbed (mg/g)} \times 100 \quad (11)$$

2.6. Column adsorption study

The sorption efficacy of adsorbents in continuous systems is a vital consideration for evaluating their viability in industrial applications. Figure 1 illustrates the fixed-bed column layout at the laboratory scale. A vitric column of 5 cm in diameter and 120 cm in height was included in the apparatus. Glass fleeces were used at both ends of the column to avert adsorbent loss in the treated water. The column was filled with a predetermined concentration of adsorbent. De-ionized (DI) water was employed to saturate the column, facilitating the release of trapped gases between the adsorbent particles. A peristaltic pump (Longer, China) was employed to transfer Pb (II) from the base of the column through the adsorbent [25].

All residual adsorbent was removed from the treated effluent utilizing a membrane filter (0.45 μm). The operating parameters for the column study were optimized by a systematic set of tests to achieve maximal Pb (II) removal. The pH was initially sustained at 6, the Pb (II) content fluctuated between 50 and 100 mg/L, the bed height was modified between 10 and 20 cm, and the mass of PTC 500 used varied between 50 and 150 g. The flow rate was modified to range from 8.33 to 12.50 mL/min. The volume of the solution varied between 12,000 and 18,000 mL. The interaction duration ranging from 10 to 1440 minutes was evaluated and enhanced.

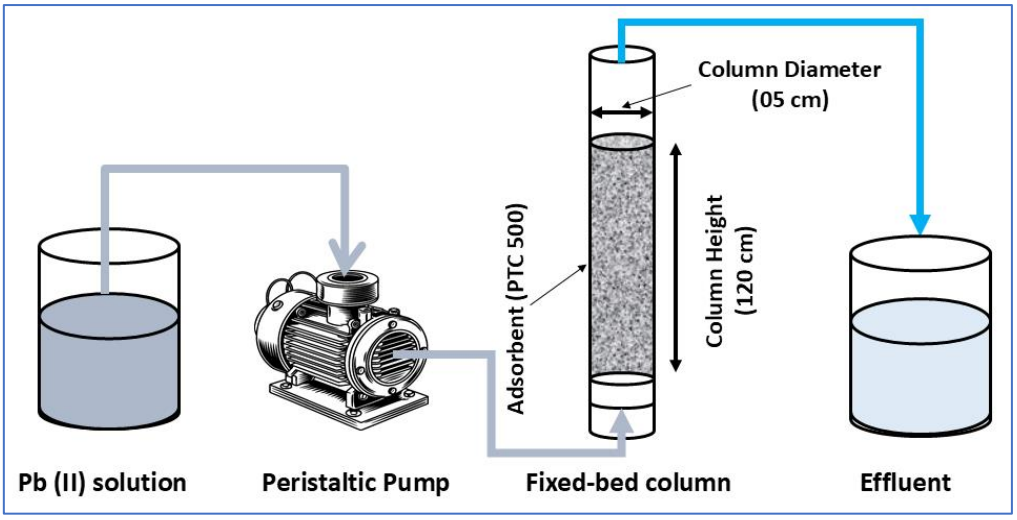

Figure 1. Schematic of Pb (II) adsorption column setup.

2.7. Breakthrough curve study

The buckling behavior of Pb (II) on PTC 500, selected for its greatest adsorption in batch investigations, was characterized by the breakthrough curve (50%) as depicted in the C_t/C_o vs T graph, according to [26]. The mass adsorbed of Pb (II) (mg/g) was calculated using the area (A) under the breakthrough curve and the flow volume (mL) according to Eqs (12)–(14).

$$\text{Total mass adsorbed}: \ q\ (0.5) = \ Q \int_{t=0}^{t=0.5} \left(1 - \frac{C_t}{C_o}\right) d_t \tag{12}$$

$$\text{Adsorption capacity:}\ q_{ac} = {}^{q_{0.5}}/_{W} \tag{13}$$

$$\text{Effluent volume: V} \ = \ \text{Qt} \tag{14}$$

where 'W' indicates the mass of PTC (g) filled in the column. At a specified flow rate, pH, and bed height, a predetermined quantity of PTC was introduced into the column, followed by the injection of a suitable volume of Pb (II) solution from the bottom. An automated collector collected the wastewater, while a ball valve equipped with a flowmeter regulated and monitored the flow rate. The removal efficiencies, adsorption capacity, and kinetics were measured utilizing the numerical nonlinear models of Clark, Thomas, Yoon-Nelson, and Bohart-Adams, as delineated in Eqs (15)–(17).

$$\text{Clark Model:}\ {}^{C_t}/_{C_O} = \ (1 \ + (n/A)\ \exp(-K_C \ \times t))^{-1/n} \tag{15}$$

$$\text{Thomas model:}\ {}^{C_t}/_{C_O} = \ 1/(1 \ + \ \exp(K_{TH} \times (q_o \times M - \ Q_t\ ))) \tag{16}$$

$$\text{Yoon} - \text{Nelson model:}\ {}^{C_t}/_{C_O} = \ 1/(1 \ + \ \exp(K_{YN} \times (t - \ \mathcal{T}\ ))) \tag{17}$$

$$\text{Bohart} - \text{Adams model:}\ {}^{C_t}/_{C_O} = \ 1/(1 \ + \ \exp(\frac{K_{BA}\, Z\, q_O}{Q} - \ K_{BA}\, C_O t)) \tag{18}$$

where 'C_t' is effluent concentration (mg/L), 'C_0' is initial concentration (mg/L), 'k' is rate constant, 't' is time (min), 'A' is adsorption capacity constant and flow rate, 'n' is sorption intensity, 'q_0' is

adsorption capacity (mg/g), 'M' is adsorbent mass (g), 'Q' is flow rate (mL/min), and 'τ' is time for 50% breakthrough (min).

3. Result and discussion

Scanning electron microscopy (SEM), EDX spectra illustrated in Figures 2(a)–(c), and point of zero charge (pH_{pzc}) measurements depicted in Figure 3 were employed to investigate the physicochemical properties of parthenium-derived biochar [27]. The figure displays the SEM of the structure, illustrating its heterogeneity and porosity characterized by elongated channels, cracks, and voids. The biochar's macroporous and mesoporous structure, characterized by a pore size ranging from around 0.1 to 12.16 µm, enhances the transport of metal ions. The capacity for heavy metal adsorption is augmented by the presence of several active sites, as shown by the irregular surface morphology [28].

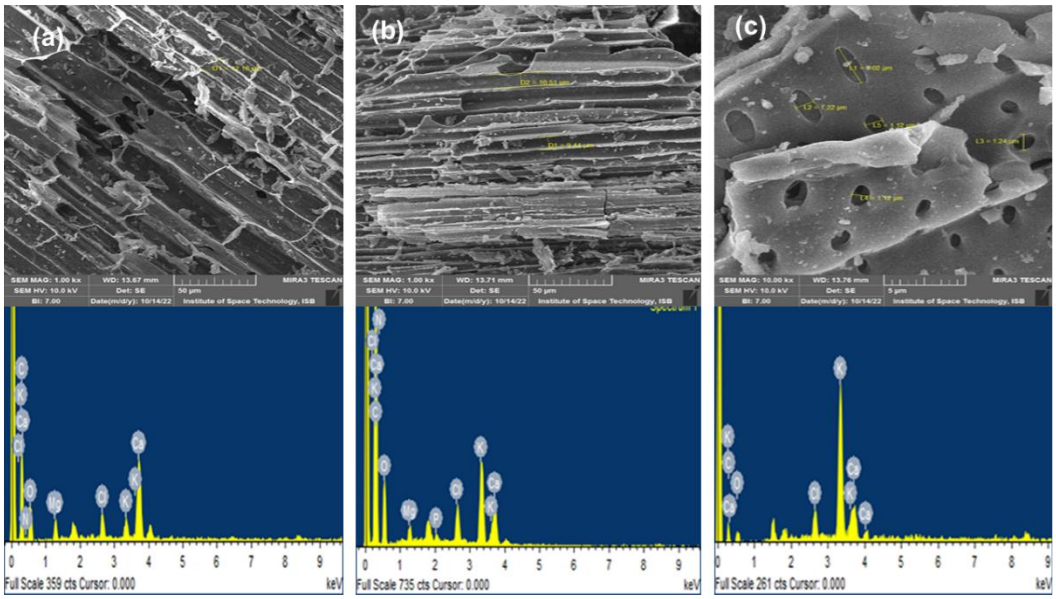

Figure 2. SEM photographs and EDX spectra of biochars derived from *Parthenium hysterophorus* (PTC 300) (a), (PTC 500) (b), and (PTC 700) (c).

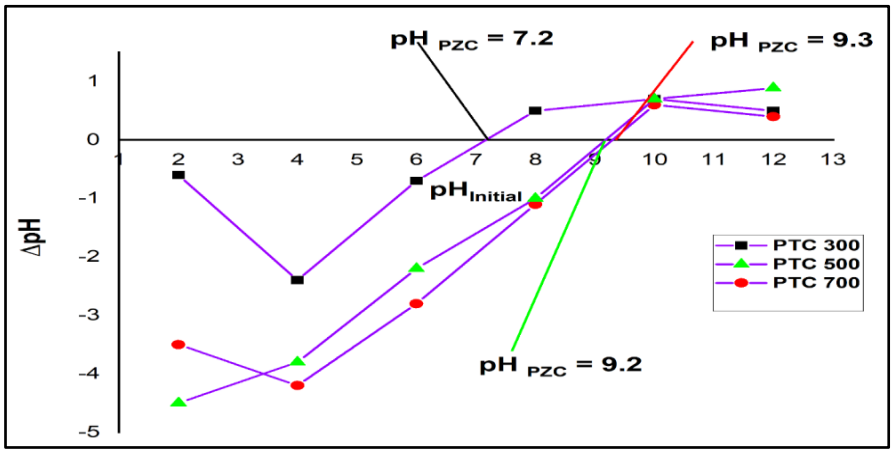

Figure 3. pH_{PZC} spectra of biochars (PTC 300, PTC 500, and PTC 700) derived from *Parthenium hysterophorus* at three temperatures (300, 500, and 700ºC).

PTC 500 possesses a pH_{pzc} of 9.2, indicating that when the solution's pH falls below this threshold, the biochar's surface exhibits a net negative charge. The adsorption studies were conducted at a working pH of 6.0, which is below the pH_{pzc}. The mostly negative charge of the biochar surface facilitated the electrostatic attraction of positively charged Pb (II) ions. The positive surface charge characteristics of PTCs support their capacity to remove cationic metals from water [29].

Despite variations attributed to pyrolysis temperature, the FTIR analyses of PTC 300, PTC 500, and PTC 700 biochar, both pre- and post-Pb (II) adsorption (Figure 4), together corroborate the significance of oxygen-containing functional groups in lead binding. The participation of hydroxyl, carboxyl, and quinone moieties in Pb (II) complexation was evidenced by the O–H stretching at 3306 cm^{-1} shifting to lower wavenumbers with diminished intensity at 3230 cm^{-1}, the C=O/C=C bands near 1564 cm^{-1} broadening to 1566 cm^{-1}, and the C–O vibrations at 1106 cm^{-1} decreasing to 1033 cm^{-1} [30]. A novel band at 657 cm^{-1} also indicated the production or precipitation of Pb–O bonds.

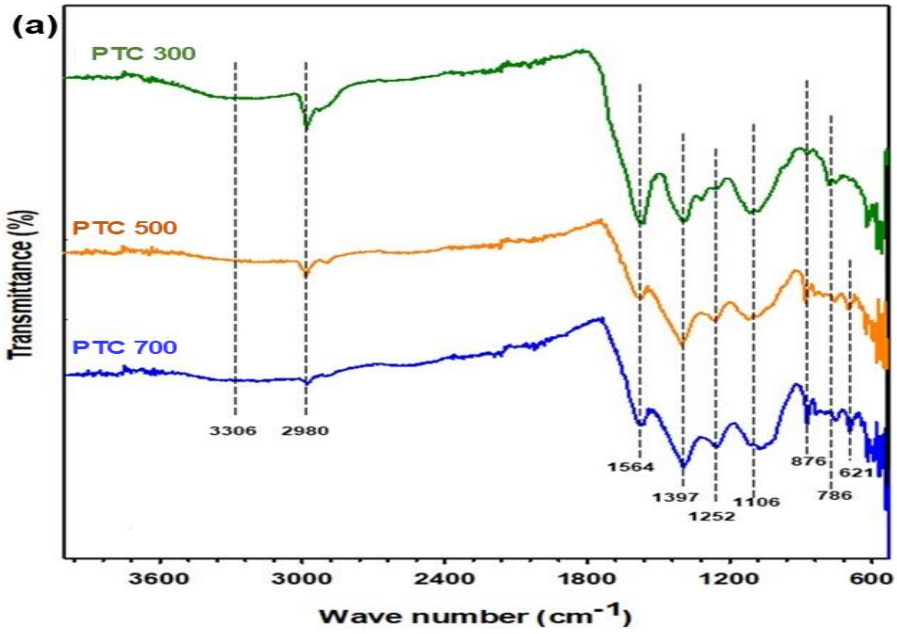

Figure 4. FTIR spectra of biochars before adsorption of Pb (II) (PTC 300, PTC 500, and PTC 700) derived from *Parthenium hysterophorus* at three different temperatures (300, 500, and 700ºC).

The presence of hydroxyl, carboxyl, and phenolic groups was validated by the PTC 500, at 2080 with carbon stretching attributed to Pb adsorption, where broad O–H bands (cm^{-1}) shifted to 3230 upon Pb loading, C=O stretching (1796 cm^{-1}) and aromatic/COO^- peaks (1566 cm^{-1}) exhibited significant alterations, and C–O stretching (1033 cm^{-1}) diminished. Vibrations of Pb–O were attributed to new bands below 600 cm^{-1} [31].

The O-H absorption at 3230 cm^{-1} for PTC 700 diminished post-adsorption, the C=O band at 1796 cm^{-1} and the COO^-/aromatic C=C peaks at 1566 cm^{-1} shifted, and the C–O peak at 1106 cm^{-1} exhibited reduced intensity. New absorptions also appeared in the region below 600 cm^{-1}, further signifying the formation of Pb–O bonds. The FTIR results across all pyrolysis temperatures indicate that the primary active sites for Pb (II) adsorption via complexation, ion exchange, and surface precipitation consistently include hydroxyl, carbonyl, carboxyl, and phenolic groups. The minor discrepancies in

peak positions and intensities indicate the alterations in the structure and chemistry of biochar as the pyrolysis temperature increases [32].

3.1. Batch adsorption study

3.1.1. Effects of adsorption parameters

The principal aspects in the adsorption process encompass the starting concentration of the adsorbate, the dosage of the adsorbent, the pH of the solution, and the duration of contact. Figure 5(a)–(d) demonstrates the influence of these factors on the removal and adsorption efficacy of PTCs for Pb (II) from water. Figure 5(a) depicts the influence of initial Pb (II) concentration on the adsorption capabilities of three PTCs. PTC 500 demonstrated a peak adsorption capacity of 7.16 mg/g at an initial concentration of 15 mg/L for Pb (II). The removal effectiveness of all PTCs diminished after 10 mg/L, presumably due to the colonization of functional sites on the PTC surface by Pb (II) ions and interactions with adsorbed functional groups. A prevalent pattern noted among all PTCs reveals that Pb (II) adsorption escalates with increased starting concentrations, ascribed to intensified interactions between the adsorbent and adsorbate molecules. As the concentration of PTCs rises, the adsorption of Pb (II) diminishes (Figure 5(b)), owing to the restricted availability of PTCs sites for adsorption [33]. The adsorption capabilities of the PTCs at a minimum dosage of 0.2 mg/L were as follows: PTC 500 had a concentration of 20.40 mg/g, PTC 700 followed with 19.95 mg/g, and PTC 300 had 11.60 mg/g. This arose from the multitude of active spots on the surface of PTC 500.

The adsorption of Pb (II) reached its zenith at pH 6, maintained relative stability until pH 8, and thereafter diminished, as illustrated in Figure 5(c), due to excellent adsorption conditions and limited surface areas of PTCs [34]. The decrease noted beyond pH 8 can be ascribed to the increased precipitation of $Pb(OH)_2$ on the surfaces of PTCs, in conjunction with cation exchange [35,36].

The adsorption capabilities were quantified as 6.23 mg/g for PTC 500, 5.84 mg/g for PTC 700, and 5.48 mg/g for PTC 300. The peak adsorption of Pb (II) for PTCs transpired at pH 6, signifying the involvement of electromagnetic processes in conjunction with additional adsorption mechanisms, including surface complexation, ion exchange, and precipitation [37] . Figure 5(d) illustrates the effect of contact period on the percentage of Pb (II) elimination and the amount adsorbed by various PTCs. The maximum adsorption of Pb (II) transpired within 45 minutes of contact time. Following the fast adsorption phase, a more gradual phase ensues until equilibrium is attained. The findings demonstrate that the pace of chemical interaction between Pb (II) and PTCs is swift, achieving maximum adsorption within a short duration of 45 minutes. PTC 500 demonstrated superior adsorption capacity relative to PTC 300 and PTC 700. Co-precipitation may expedite the fast elimination of Pb (II) [38]. During the sluggish phase, the interaction between Pb (II) and the PTCs surface may entail intra-particle mobility [39].

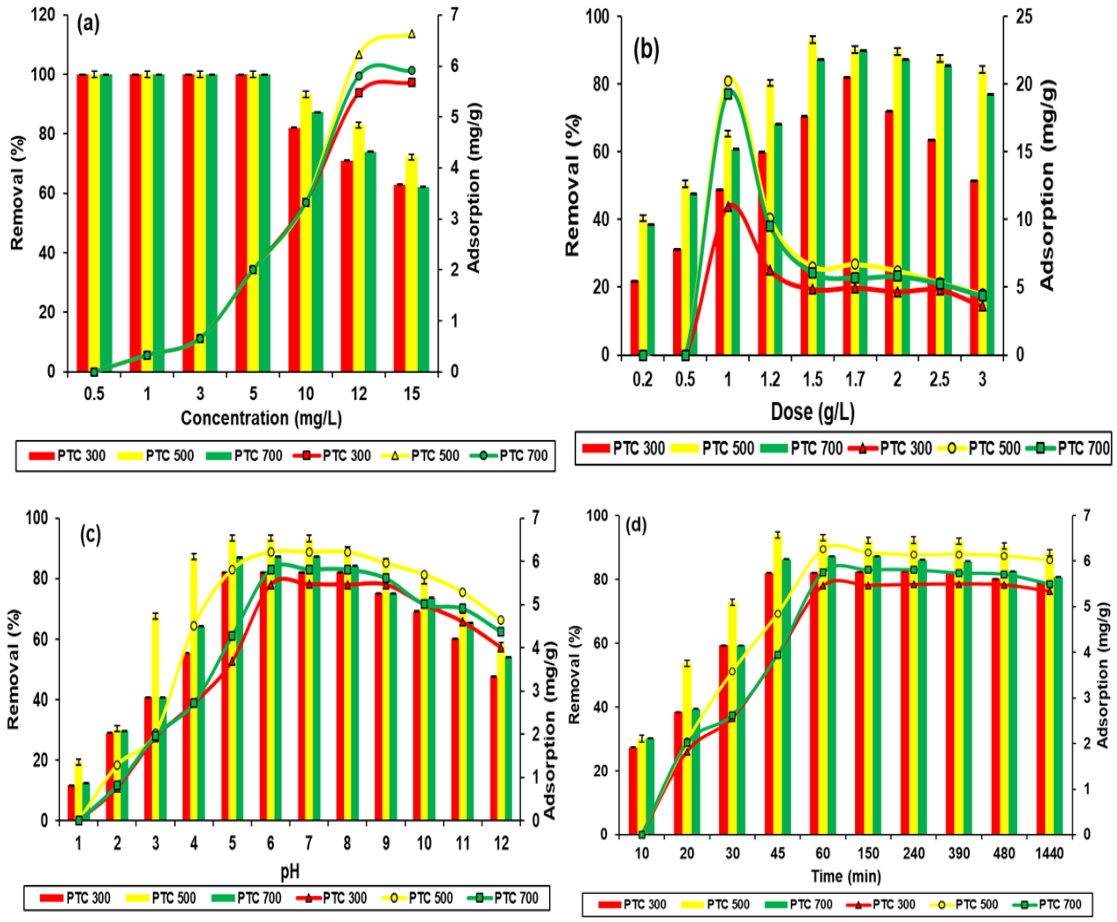

Figure 5. Effects of (a) Initial concentration, (PTC dose =1.5 g/L, pH = 6, Time = 1440 min, Temp = 25°C); (b) PTC dose (pH = 6, Conc of Pb (II) = 10 mg/L, Time = 1440 min, Temp = 25°C) (c), pH (PTC dose = 1.5 g/L, Conc of Pb (II) = 10 mg/L, Time = 1440 min, Temp = 25°C); and (d) contact time (PTC dose = 1.5 g/L, pH = 6, Conc of Pb (II) = 10 mg/L, Temp = 25°C) on removal and adsorption of Pb (II) by biochars (PTC 300, PTC 500, PTC 700). The Bar chart represents Removal % and the curve chart represents Adsorption (mg/g).

3.1.2. Isothermal study

The correlation coefficients (R^2) in Table 1 and Figure 6 (a)–(d) demonstrate that the adsorption data for PTC 500 aligns well with the Langmuir and Freundlich isotherm models, but does not adhere to the Temkin and D-R models. Langmuir estimated a maximum adsorption capacity (Q_{max}) of 18.57 mg/g for PTC 500, which notably exceeded the capacities of PTC 300 (12.37 mg/g) and PTC 700 (12.94 mg/g). The 1/n values forecasted by the Freundlich model for all PTCs exceeded 1, signifying favorable adsorption of Pb (II). The Temkin model indicated that the B values for all PTCs were below 8 kJ/mol, signifying that the adsorption process was classified as physisorption [40]. Consistent with the Langmuir demonstration, the Q_D values forecasted by the Dubinin-Radushkevich model were much greater for PTC 500 (7.55 mg/g) than for PTC 700 (6.63 mg/g) and PTC 300 (6.38 mg/g).

Table 1. Parameters for Pb (II) adsorption onto biochars (PTC 300, PTC 500, and PTC 700) determined using isothermal and kinetic models.

Isothermal models												
	Langmuir			Freundlich			Temkin			Dubinin Radushkevich		
	R^2	Q_{max} (mg/g)	K_L (l/mg)	R^2	1/n	K_F (mg/g)	R^2	B (kJ/ mol)	A (l/mg)	R^2	Q_D (mg/g)	ε (J/mol)
PTC 300	0.992	12.37	0.07	0.977	1.42	0.98	0.935	1.83	1.61	0.971	6.38	1
PTC 500	0.994	20.40	0.04	0.981	1.28	0.93	0.903	2.14	1.48	0.970	7.55	1
PTC 700	0.988	12.94	0.07	0.968	1.41	1.00	0.926	1.91	1.59	0.972	6.63	1
Kinetic models												
	Pseudo-first-order			Pseudo-second-order			Elovich			IPD		
	R^2	q_e (mg/g)	k_1 (min^{-1})	R^2	q_e (mg/g)	k_2 (g/mg-min)	R^2	α (mg/g-min)	β (g/mg)	R^2	C (mg/g)	k_1 (mg/g-$min^{-0.5}$)
PTC 300	0.921	5.52	0.04	0.795	5.83	0.011	0.490	8.31	1.56	0.18	3.73	0.067
PTC 500	0.938	6.19	0.05	0.789	6.51	0.012	0.439	25.58	1.57	0.14	4.46	0.064
PTC 700	0.899	5.75	0.04	0.766	6.06	0.010	0.455	10.19	1.53	0.15	3.93	0.066

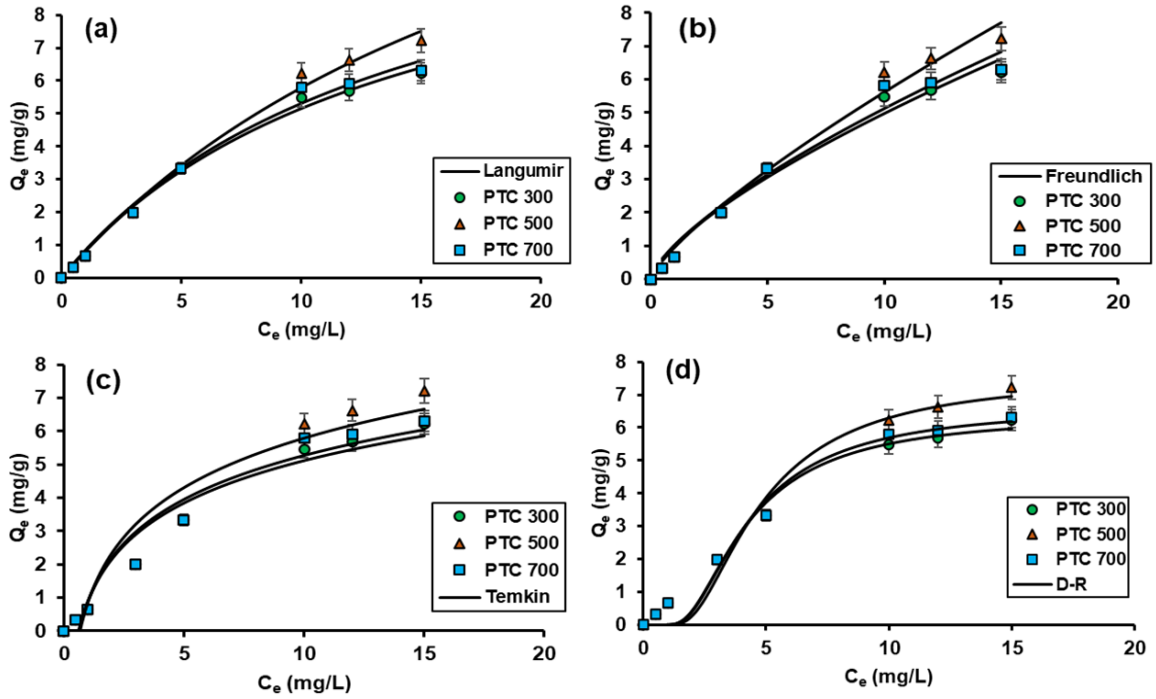

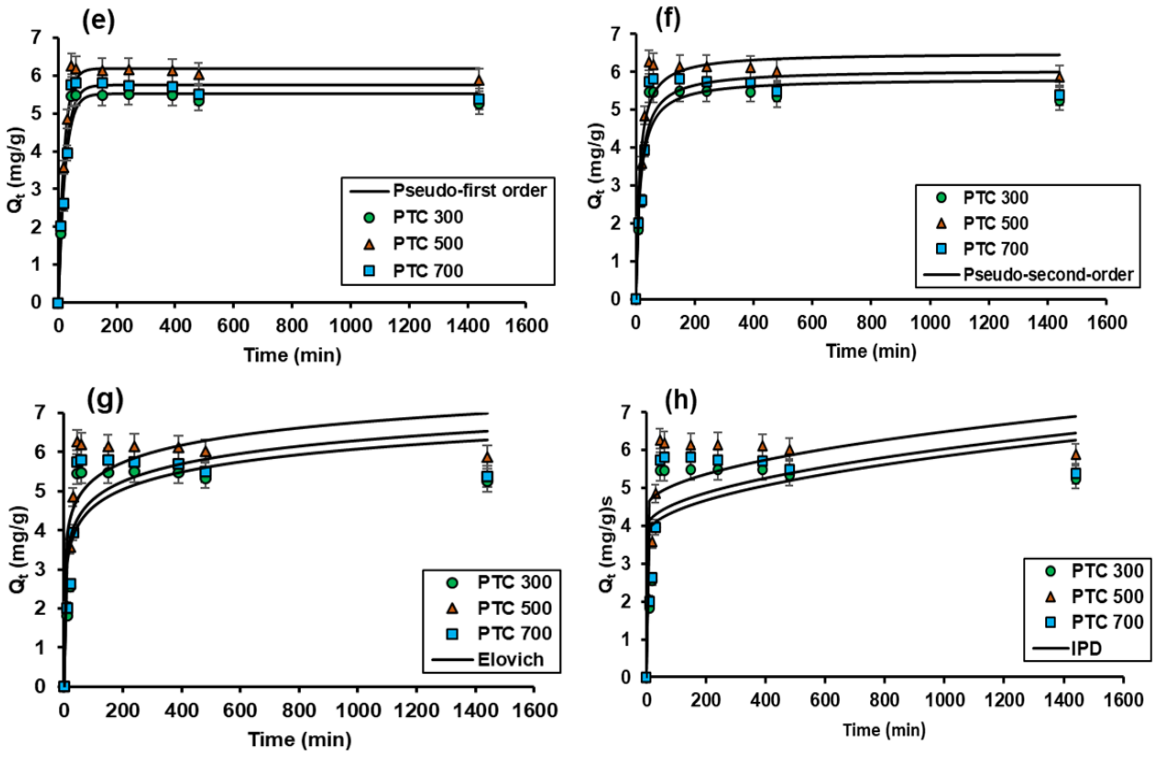

Figure 6. Non-linear fittings of isothermal models. (a) Langmuir, (b) Freundlich, (c) Temkin, (d) Dubinin Radushkevich (D-R), and kinetic models, (e) pseudo-first-order, (f) pseudo-second-order, (g) Elovich model, and (h) intra-particle diffusion, on Pb (II) adsorption onto PTC 300, PTC 500, and PTC 700.

The findings of the isotherm models demonstrated that PTC 500 displayed the greatest adsorption of Pb (II) relative to PTC 300 and PTC 700. The elevated R^2 and Q_{max} values of the Langmuir isotherm signify a homogeneous monolayer adsorption process, whereas the active sites on the surface exhibit numerous significant benefits for adsorption [41]. The Temkin isotherm model further underscores the uniform distribution of binding energies throughout the PTCs [42]. In contrast, the Freundlich, Temkin, and Dubinin-Radushkevich models indicate heterogeneous adsorption, reflecting significant variability in the surfaces of the PTCs. The adsorption of Pb (II) on PTCs appears to include multiple mechanisms, as evidenced by the well-fitted isothermal models [43], which include pore-filling diffusion (Dubinin-Radushkevich model), multilayer adsorption (Freundlich model), and monolayer adsorption (Langmuir model).

We examined the adsorption of Pb (II) utilizing four kinetic models: Intra-particle diffusion (IPD), pseudo-second order (PSO), Elovich, and pseudo-first order (PFO). Figure 6(e)–(h) illustrates the curve fittings for each model, while Table 1 lists the associated parameters. The R^2 values, ranging from 0.144 to 0.938, demonstrated that the PFO, PSO, and Elovich models are appropriate for the Pb (II) kinetic adsorption data. However, the results were inconsistent with the intraparticle diffusion concept, as evidenced by an R^2 value below 0.5. In the assessment of the PTC series, PTC 500 exhibited enhanced estimated equilibrium adsorption capacity (q_e) values for PFO and PSO, measured at 6.51 and 6.19 mg/g, respectively, in contrast to PTC 300 and PTC 700. Furthermore, PTC 500 exhibited an elevated adsorption rate of 20.40 mg/g-min. PTC 500 demonstrated superior adsorption capacity for Pb (II) relative to PTC 300 and PTC 700, as evidenced by kinetic results consistent with isothermal models. This signifies the participation of several unique adsorption mechanisms. The robust

connection of the kinetic data with the PFO and PSO models demonstrated that Pb (II) is adsorbed onto all PTCs, especially PTC 500, by a mix of physisorption and chemisorption processes [44]. The maximum adsorption level observed in this investigation, in comparison to other biochars employed for the same Pb (II) removal from aqueous solutions, indicated a higher performance in this research (Table 2).

Table 2. Comparison of the adsorption capacity of biochar derived from *Parthenium hysterophorus* at 500ºC (PTC 500) from this study with other reported studies.

Biochar	Pyrolysis temperature (℃)	Adsorption capacity (mg/g)	Reference
Bamboo, bagasse, and tire biochar	105	0.15	[13]
Wheat straw powder biochar	350	9.95	[45]
Coffee husk biochar	350	13.08	[44]
Parthenium hysterophorus biochar	500	18.41	[10]
Prosopis wood biochar	400	18.72	[32]
Parthenium hysterophorus biochar	500	20.40	This study

3.1.3. Industrial wastewater and reusability study

At this stage of the inquiry, the specified operational parameters in Section 2.3 were selected to remove Pb (II) from actual industrial wastewater through a batch adsorption experiment. The results demonstrated a 97% elimination of Pb (II). Additionally, a significant decrease in other conventional wastewater pollutants was noted, as demonstrated in Table 3. The physical structure of PTC 500 successfully caught total suspended solids (TSS), resulting in a 70% reduction. It comparably removed organic pollutants and total dissolved solids (TDS) through adsorption and ion exchange mechanisms. Additional treatment of industrial wastewater is required to meet the permitted limits established by NEQS for biological oxygen demand (BOD) and chemical oxygen demand (COD) characteristics [46].

Table 3. Real industrial wastewater characteristics before and after adsorption through PTC 500.

Parameters	NEQS	Inlet real wastewater	After adsorption	% Removal
COD (mg/L)	400	3,220 ±1.2	2,049 ±2	55%
BOD (mg/L)	250	1,440 ±1.02	734.4 ±2	49%
TDS (mg/L)	3,500	2,236 ±2.12	1,788.8 ±1	20%
pH	6-9	6.28±0.18	6 ±0.1	--
EC (Ds/m)	N/A*	3.40±0.22	3.45±1	--
TSS (mg/L)	400	612 ±0.1	184 ±0.1	70%
Pb (mg/L)	0.5 (mg/L)	0.85 ±0.01	0.025 ±0.01	97%

*N/A = Not available, NEQS = National Environmental Quality Standards.

Five successive adsorption–desorption cycles were conducted to comprehensively assess the regeneration and reusability of the synthesized PTC 500 utilizing five distinct 0.1N regenerative agents (CH_3COOH, H_2SO_4, HCl, NaOH, NaCl). Acidic eluents, including HCl, H_2SO_4, and CH_3COOH, were employed to promote proton exchange with adsorbed Pb (II) ions and to dissociate metal-functional group complexes through the protonation of oxygen-containing surface groups [47]. NaCl was employed to assess the reversibility of ion-exchange and electrostatic interactions by competitively displacing Pb (II) ions with Na^+ ions [48]. To evaluate the adsorbent's stability under acidic conditions and the desorption behavior associated with variations in surface charge and metal speciation, NaOH was introduced [49]. Prior to reuse, the Pb (II)-imbued PTC 500 was rinsed with deionised water, treated with the requisite reagent after each sorption cycle, and subsequently dried in an oven at 80°C.

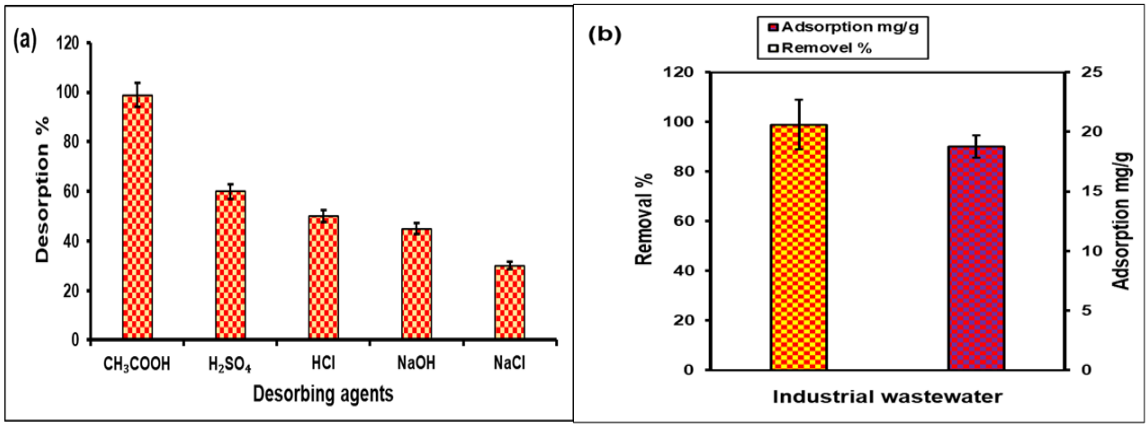

Figure 7. (a) Desorption of Pb (II) by different desorbing agents, and (b) Removal and adsorption of Pb (II) from industrial wastewater by biochar (PTC 500).

Figure 7(a) illustrates the fluctuation in regeneration efficacy based on the reagent utilized. The PTC 500 exhibited an adsorption capacity for CH_3COOH cleaning of 98.9% in the initial cycle, which progressively diminished to 95% in the second cycle and further to 86% in the third cycle. Following the fourth and fifth cycles, the regeneration efficiency was about 79% and 75%, respectively. H_2SO_4 demonstrated reduced regeneration efficiency, sustaining 60% after five cycles, while HCl, NaOH, and NaCl showed significant retention of adsorption capacity at 50%, 45%, and 30% respectively, likely attributable to considerable structural modifications and the depletion of surface functional groups [50]. The most substantial reduction in reusability occurred after CH_3COOH treatment; following five cycles, capacity decreased from 20.40 to 15.3 mg/g, indicating an efficiency of just 20%. The PTC 500 successfully removed 95% of Pb (II) from wastewater, exhibiting an adsorption capacity of 18.74 mg/g (Figure 7(b)). The unexpectedly diminished adsorption capacity of PTC 500, recorded at below the anticipated value of 20.40 mg/g, may be ascribed to the conflicting effects of several soluble cations in wastewater, as indicated by increased electrical conductivity (EC) and total dissolved solids (TDS) levels. The diminished capacity for Pb (II) adsorption in actual wastewater, compared to synthetic solutions, is attributed to the presence of competing ions and the heightened ionic strength of the matrix. Elevated TDS and EC values indicate an increase in dissolved ions such as Ca^{2+}, Mg^{2+}, Na^+, and K^+, which may compete with Pb (II) for ion-exchange sites and oxygen-rich functional groups on the charcoal surface. Furthermore, elevated ionic strength can mask the electrostatic interactions between Pb (II) and the negatively charged functional groups, resulting in diminished adsorption efficiency.

The interaction of these elements likely results in a reduction in Pb (II) absorption in complex wastewater systems [51]. Notably, following treatment with PTC 500, the Pb (II) concentration in the treated wastewater was 0.025 mg/L, which is below the permissible limit of 0.5 mg/L set by Pak-EPA (2000).

3.1.4. Column study

A fixed-bed column incorporated an adsorbent methodically positioned within its framework. A Pb (II) solution with a specified influent concentration was supplied at a steady flow rate and sustained under strictly regulated circumstances. The effluent concentration was consistently checked at regular intervals over time. The adsorbent exhibited a substantial capacity for holding Pb (II) molecules, leading to a significantly low effluent concentration. Nevertheless, the presence of Pb (II) in the effluent could be ascribed to the gradual saturation of the adsorption sites at the column's entrance over time. As saturation advanced through the bed, the effluent concentration gradually increased, approaching the influent concentration, indicating the onset of column collapse. Figure 8 depicts the conventional breakthrough curve, generated by graphing the normalized effluent concentration (Ct/C_0) against time. This curve depicts the operational characteristics of the adsorption column and its efficient mass transfer performance [52].

In the column experiment, the PTC 500 was the most efficient adsorbent according to the results derived from the batch study. This study defined the breakthrough point ($t_{0.5}$) as the moment when the effluent concentration (C_t) reached 50% of the influent concentration ($C_t/C_0 = 0.5$) [53]. The different operating conditions were analyzed as detailed in Table 4.

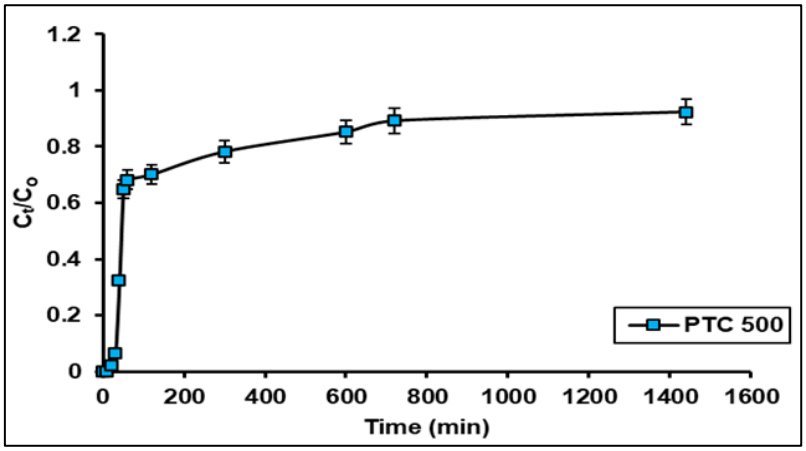

Figure 8. Breakthrough curves for Pb (II) adsorption on PTC 500 (pH 6, time 1440 min, temp = 25°C, Bed height (mass of adsorbent) = 10 cm (50 g), initial concentration of Pb (II) = 100 mg/L, Flow rate = 8.33 mL/min). Solid line = model calculation; data marks = experimental measurements.

Table 4. Column parameters with different bed heights, flow rates, and vent concentration.

Vent Conc. (mg/L)	Flow rate (mL/min)	Bed Height (cm)	Mass of PTC 500 (g)	Breakthrough curve point (50%) (min)	Treated volume (mL)	Adsorption capacity (mg/g)
50	8.33	10	50	17.6	11,999	2.94
70	8.33	10	50	24.6	11,999	4.09
100	8.33	10	50	49.0	11,999	8.16
100	8.33	10	50	49.0	11,999	8.17
100	10.83	10	50	32.63	15,595	7.16
100	12.50	10	50	20.83	18,000	5.21
100	8.33	10	50	48.0	11,999	8.00
100	8.33	15	100	99.58	11,999	8.30
100	8.33	20	150	155.3	11,999	8.64

3.1.5. Influence of variables

Investigations were performed at a pH of 6 using PTC 500, with a column bed height between 10 and 20 cm, and a vent concentration of 50 to 100 mg/L, to analyze the impact of flow rate on the adsorption of Pb (II) in the column, as depicted in Figure 9(a). The flow rates in a continuous fixed-bed column experiment affected the removal efficiency of Pb (II). We investigated the elimination of Pb (II) by assessing the impact of various flow rates specifically 8.33, 10.83, and 12.50 mL/min while keeping bed heights at 10 cm and metal concentrations at 100 mg/L. A decrease in flow rate from 12.5 to 8.33 mL/min resulted in an increase in breakthrough and fatigue times. An increased flow rate reduced the contact time of the Pb (II) solution, compromising its adsorption capacity by the adsorbent. As the flow velocity decreased, the residence time of the solution increased, facilitating its permeation via the pores [54]. As the flow velocity diminished, the adsorption capacity increased from 5.21 to 8.17 mg/g, as indicated in Table 4. The findings demonstrated the need of regulating the influent flow rate and contact duration to optimize the removal of Pb (II) and prevent premature saturation, thus ensuring the best performance of the fixed-bed system [55]. The breakthrough curve of Pb (II) was assessed at a concentration of 100 mg/L and a flow rate of 8.33 mL/min, employing bed heights of 10 cm (50 g), 15 cm (100 g), and 20 cm (150 g). The recorded suffusion and breakthrough timings demonstrated an increase with the rise in bed height from 10 to 20 cm, as depicted in Figure 9(b). The adoption of increased bed heights led to diminished effluent concentrations and prolonged saturation periods for the adsorbent, as demonstrated in Table 4. A smaller bed attained saturation more rapidly due to fewer binding sites and an enlarged surface area for metal adsorption, while a longer bed demonstrated extended functionality. Increasing bed height has been demonstrated to considerably delay breakthrough and saturation events by expanding the mass transfer zone, as indicated by the findings in [1]. The prolonged residence time facilitates enhanced reduction and adsorption processes for Pb (II). Thus, an increase in bed height results in improved efficiency in the use of adsorbents, which is consistent with findings from other studies [56]. The ideal bed height for maximizing adsorption was 10 cm, and this parameter was selected for subsequent experiments. Another study [57]

exhibited analogous adsorption patterns concerning different bed heights. We investigated the effects of varying concentrations of Pb (II) (50, 70, and 100 mg/L) on the breakthrough curve, with a flow rate of 8.33 mL/min and a bed height of 10 cm. The elevation in concentration from 50 to 100 mg/L caused a significant modification of the breakthrough curve (Figure 9(c)). The recorded break and saturation periods demonstrated a reduction in relation to the elevation of Pb (II) content (Table 4). At diminished concentrations, a larger volume of Pb (II) was required for efficient removal, and the breakthrough time extended primarily due to decreased mass transfer during the adsorption phase. The augmented adsorbate volume per unit surface area of the PTCs caused earlier saturation, hence reducing saturation time with the increase in Pb (II) concentration [58]. As the concentration of Pb (II) rose, the adsorption capacity correspondingly increased due to the accelerated saturation of the PTCs. The findings demonstrated the need of regulating the influent flow rate and contact duration to enhance the removal of Pb (II) and prevent early saturation, thus ensuring the best performance of the fixed-bed system.

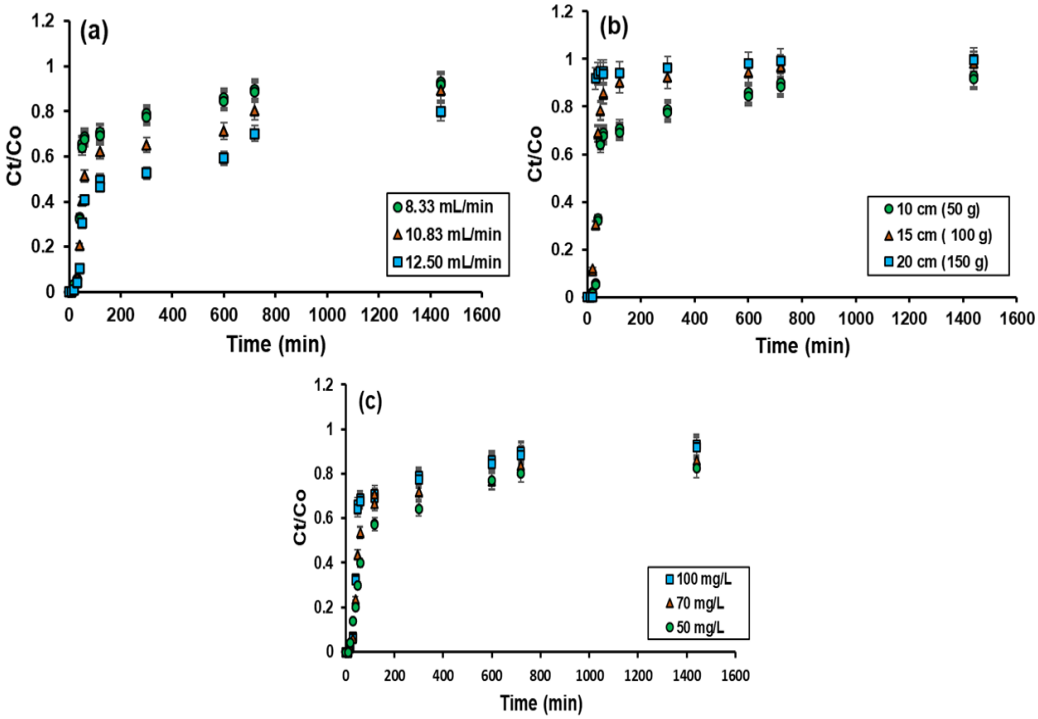

Figure 9. Effects of (a) Flow rate, (pH = 6, time 1440 min, temp = 25°C, Bed height (mass of adsorbent) = 10 cm (50 g), 15 cm (100 g), 20 cm (150 g), initial concentration of Pb (II) = 100 mg/L, 70 mg/L,50 mg/L) (b) Bed height (mass of adsorbent) (pH = 6, time 1440 min, temp = 25°C , Flow rate = 8.33 mL/min, 10.83 mL/min, 12.50 mL/min, initial concentration of Pb (II) = 100 mg/L, 70 mg/L,50 mg/L), and (c) Initial concentration of Pb (II) (pH = 6, time 1440 min, temp = 25°C, Bed height (mass of adsorbent) = 10 cm (50 g), 15 cm (100 g), 20 cm (150 g), flow rate = 8.33 mL/min, 10.83 mL/min, 12.50 mL/min, on adsorption by biochar (PTC 500).

3.1.6. Column models

The continuous mode experiment showed that an elevation in bed height resulted in a decrease in flow velocity, whereas an increased concentration of Pb (II) augmented the sorption of Pb (II) onto

PTC 500 biochar. The modeling results for column adsorption, depicted in Figure 10(a)–(l) and summarized in Table 5, demonstrated that an increase in bed height from 10 to 20 cm, a decrease in flow rate from 12.50 to 8.33 mL/min, and an elevation in initial Pb (II) concentration from 50 to 100 mg/L resulted in the Clark model being the optimal fit, as indicated by the Adjusted R ²values related to the Freundlich isotherm model. The batch adsorption investigation established that the Freundlich isotherm model accurately represented the adsorption of Pb (II) on PTCs. The Clark model asserted that the forces propelling intraparticle diffusion correspond to the transverse multilayer composition on the material's surface [59]. The rate of decrease in adsorption probability for all adsorbate molecules is linked to the probability of adherence and the degree of infiltration of the adsorbate into the adsorbent, as described in the Yoon–Nelson column model [60]. The notion that attaining equilibrium is not an instantaneous process is essential to the Bohart–Adams model. The adsorption rate is affected by the quantity of adsorbate and the residual capacity of the adsorbent [61].

Table 5. Parameters of Clark model, Y-N model, Thomas model, and Bohart–Adams model.

Clark model			
Parameters	K_c (mL/min mg)	A	R^2
Effect of column height (cm)			
10	0.16	0.81	0.97
15	0.15	0.93	0.99
20	1.13	0.96	0.99
Effect of concentration (mg/L)			
100	0.15	0.82	0.97
70	0.11	0.77	0.97
50	0.05	0.73	0.95
Effect of flow rate (mL/min)			
8.33	0.15	0.89	0.96
10.83	0.10	0.73	0.95
12.50	0.10	0.62	0.91
Y-N model			
parameters	K_{YN} (mL/min mg)	T (min)	R^2
Effect of column height (cm)			
10	10.24	49.94	0.73
15	8.07	39.90	0.83
20	6.46	29.62	0.99
Effect of concentration (mg/L)			
100	0.10	49.9	0.75
70	0.06	51.81	0.72
50	0.005	61.38	0.25
Effect of flow rate (mL/min)			
8.33	10.1	49.9	0.71
10.83	82.3	85.4	0.67
12.50	39.3	200.1	0.21

Continued on next page

Thomas model			
Parameters	K_T (mL/min mg)	q_{ac} (mg/g)	R^2
Effect of column height (cm)			
10	10.62	3.19	0.86
15	11.44	2.42	0.97
20	100.75	1.83	0.99
Effect of concentration (mg/L)			
100	10.44	3.18	0.85
70	3.54	4.87	0.77
50	055	17.04	0.75
Effect of flow rate (mL/min)			
8.33	10.48	3.29	0.85
10.83	0.48	17.40	0.68
12.50	0.33	29.39	0.68
Bohart–Adams model			
Parameters	K_{BA} (mL/min mg)	N_o (mg/L)	R^2
Effect of column height (cm)			
10	1.42	3.57	0.84
15	2.30	1.80	0.97
20	1.48	18.68	0.99
Effect of concentration (mg/L)			
100	0.06	1.55	0.86
70	3.28	1.52	0.81
50	3.29	1.07	0.54
Effect of flow rate (mL/min)			
8.33	0.06	3.46	0.85
10.83	3.02	3.42	0.60
12.50	3.02	3.42	0.56

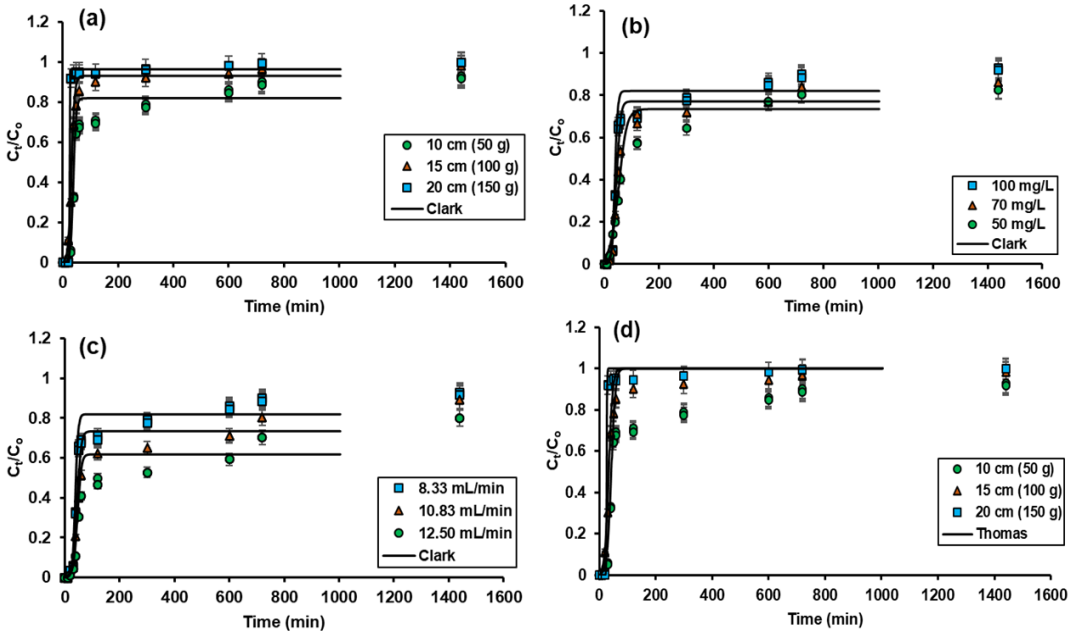

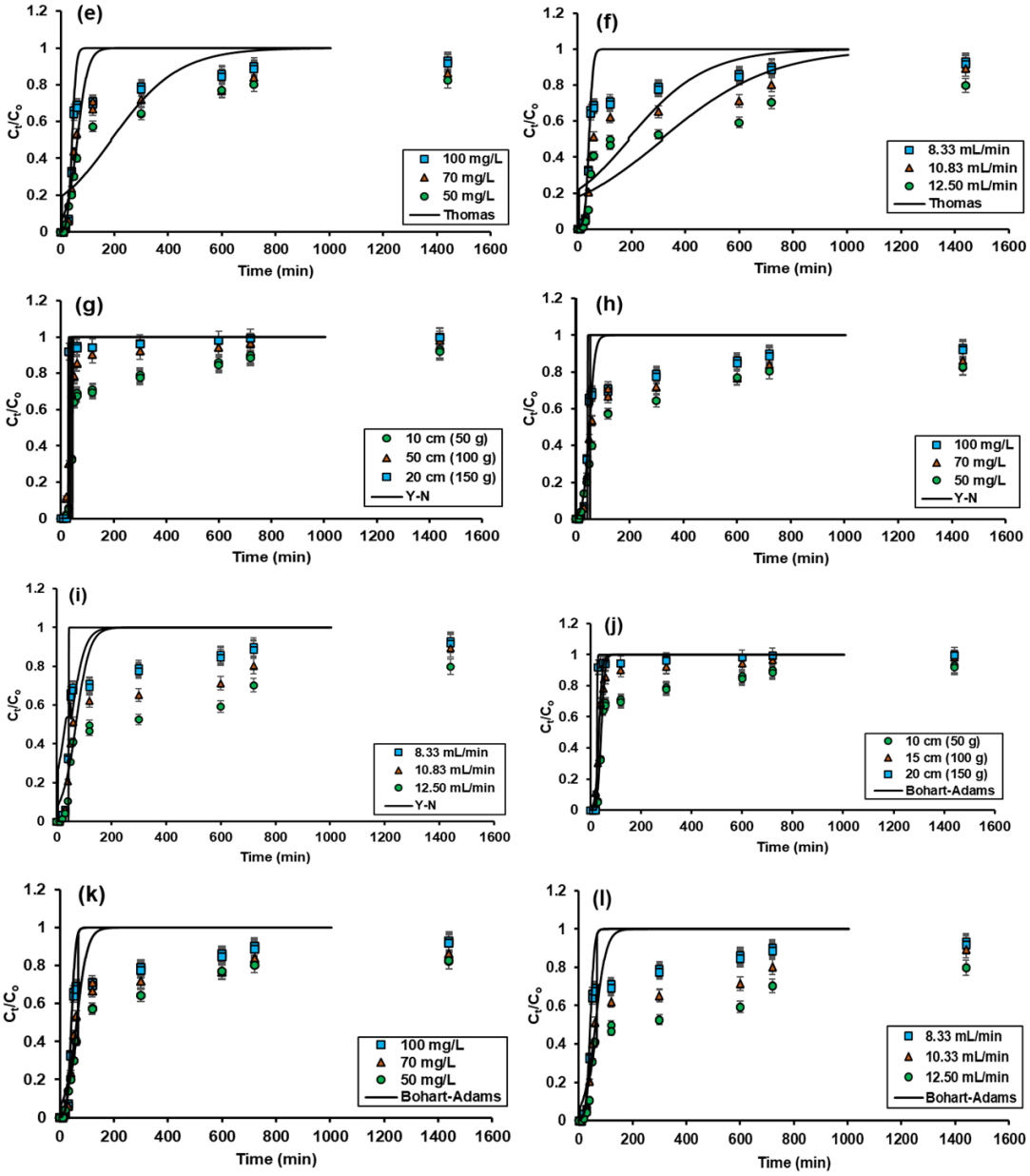

Figure 10. Non-linear fittings of breakthrough curves models, (pH = 6, time 1440 min, temp = 25°C, Flow rate = 8.33 mL/min, 10.83 mL/min, 12.50 mL/min, initial concentration of Pb (II) = 100 mg/L, 70 mg/L, 50 mg/L, bed height (mass of adsorbent) = 10 cm (50 g), 15 cm (100 g), 20 cm (150 g)) (a)–(c) Clark, (d)–(f) Thomas, (g)–(i) Yoon–Nelson, (j)–(l) Bohart-Adams on Pb (II) adsorption onto biochar (PTC 500).

The examination of the modified R^2 values revealed that the Clark model exhibited a more favorable fit under diverse situations than the Bohart–Adams (B-A) Thomas model and the Yoon Nelson (Y-N) model. With the elevation of the bed height, the Thomas model (0.99), Bohart–Adams model (0.99), Clark model (0.99), and Y-N model (0.99) demonstrated approximately equivalent fits to the column adsorption data. The elevation of initial Pb (II) concentration led to a diminished fit for the Thomas, Y-N, and B-A models, each presenting an adjusted R^2 of 0.65, in contrast to the Clark model, which exhibited a markedly superior adjusted R^2 value of 0.95. Correspondingly, as the flow rate diminished, the adjusted R^2 value for the Clark model was superior (0.96) in comparison to the

other models. The findings demonstrated that adsorption efficiency improved with greater bed height and elevated inlet Pb (II) content, as seen by the high adjusted R^2 values of 0.99 across all models. A decrease in flow rate improved the bed's adsorption capacity, thereby confirming the Clark model's efficacy in predicting adsorption behavior under these conditions [62]. The notable consistency between the Clark and improved Thomas models indicated that chemisorption at active sites, along with concentration-driven mass transfer in the column system, was the primary mechanism for the adsorption of Pb (II) on PTC 500.

3.1.7. Regeneration and treatment of industrial wastewater by column adsorption

The achievement of sustainable industrial development, in accordance with the comprehensive concept of sustainability encompassing economic, social, and environmental aspects, is largely contingent upon the deployment of efficient technologies that produce advantageous socio-economic and environmental outcomes. This advancement includes new strategies and the optimization of processes that yield optimal results while minimizing resource usage, hence providing significant benefits such as environmental sustainability and enhanced productivity. Exceptional adsorption capability, ease of reusability without substantial loss in adsorption capacity, and long-term reusability are critical features for practical applications. We employed the PTC 500 for Pb (II) adsorption, followed by desorption experiments utilizing a 0.1N CH_3COOH solution as the desorbing agent (Figure 11(b)). The regeneration cycle involved the passage of the desorbing agent through the column at a flow rate of 8.33 mL/min, with a column height of 10 cm (50 g), and a vent concentration of 100 mg/L for a specified duration. The breakthrough curve point (50%) occurred at 49 minutes. A washing phase utilizing deionized water was performed for a further 30 minutes before initiating the subsequent cycle of Pb (II) adsorption. Furthermore, following five cycles of adsorption-desorption, the PTC 500 exhibited a consistent removal efficiency exceeding 85% of its initial capacity, as illustrated in Figure 11(a). This discovery demonstrated the composite material's potential for repeated application in efficiently eliminating Pb (II) ions from wastewater streams.

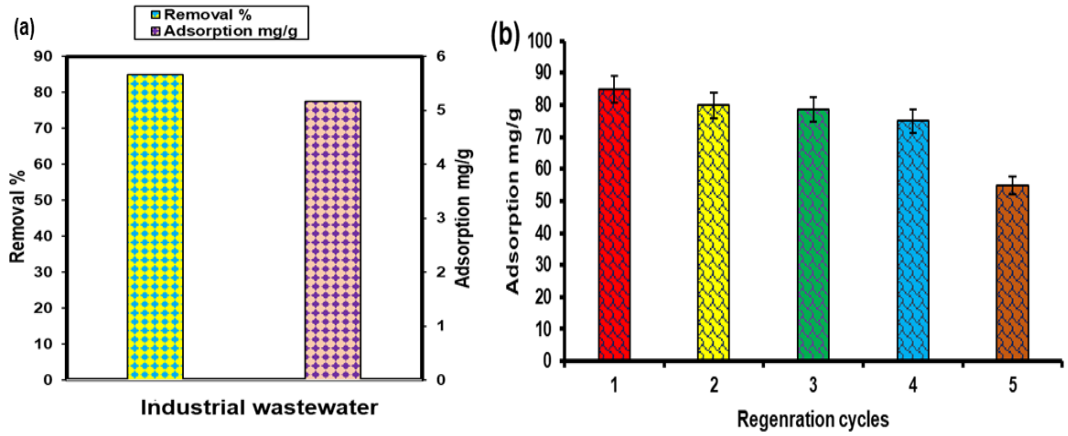

Figure 11. (a) Removal and adsorption of Pb (II) from industrial wastewater by biochar (PTC 500) through column study, and (b) Regeneration of PTC 500 in different cycles from industrial wastewater.

3.1.8. Adsorption mechanism

Despite variations attributed to pyrolysis temperature, the FTIR analyses (Figure 12(a, b)) of PTC 300, PTC 500, and PTC 700 biochar, pre- and post-Pb (II) adsorption, collectively substantiated the involvement of oxygen-containing functional groups in lead binding. The participation of hydroxyl, carboxyl, and quinone groups in Pb (II) complexation was evidenced by the O–H stretching at 3306 cm^{-1} migrating to lower wavenumbers with diminished intensity at 3230, while the C=O/C=C bands near 1564 cm^{-1} broadened to 1566 [63].

Following the adsorption process, the aliphatic stretching peak and the C–O vibrations at 1106 cm^{-1} diminished to 1033, signifying the formation of a complex between Pb (II) and the surface of PTCs. Furthermore, PTC 500 demonstrated an elevated concentration of C = C_π [64]. The post-adsorption FTIR measurements indicated that the elimination of the 2980 cm-1 signal is associated with the establishment of the C_π—Pb bond [65].

$$2Pb^{+2} + 2(C = C\pi - H_3O^+) \rightarrow 2(C = C\pi - Pb) + 2H_3O^+$$

When Pb (II) approaches an oxygen-containing group (–OH, –COOH on PTCs), the oxygen transfers a lone pair of electrons to the vacant orbital of Pb (II), resulting in the formation of a coordinate (dative) covalent bond. The bond arises from oxygen (base) giving electrons, and Lead (acid) accepts electrons to give a Lewis acid-base mechanism [66].

$$Pb^{+2} + RCOOH + H_2O \rightarrow RCOPb + H_3O^+$$

$$Pb^{+2} + ROH + H_2O \rightarrow ROPb + H_3O^+$$

Lead (II) interacts with minerals such as carbonates, phosphates, and hydroxides in biochar to produce insoluble precipitates of $PbCO_3$, $Pb_3(PO_4)_2$, and $Pb(OH)_2$ [67].

$$Pb^{+2} + OH^- \rightarrow Pb(OH)_{2(s)}$$

$$Pb^{+2} + CO_3^{-2} \rightarrow PbCO_{3(s)}$$

$$Pb^{+2} + PO_4^{-3} \rightarrow Pb_3(PO_4)_{2(s)}$$

A novel band at 657 cm^{-1} also indicated the production or precipitation of Pb (II). The involvement of hydroxyl, carboxyl, and phenolic groups was validated by the PTC 500, at 2080, indicating carbon stretching attributed to Pb adsorption. Notably, broad O–H bands (cm^{-1}) shifted to 3230 upon Pb (II) loading, while C=O stretching (1796 cm^{-1}) and aromatic/COO^- peaks (1566 cm^{-1}) exhibited significant alterations, and C–O stretching (1033 cm^{-1}) diminished. New bands below 600 cm^{-1} were attributed to Pb–O vibrations. The surface of PTCs consists of exchangeable cations, such as K^+, Na^+, Ca^{2+}, Mg^{2+}, and H^+, which are loosely bound to negatively charged functional groups (–COO^-, –OH^-, phenolic) [65]. As Pb (II) ions in the solution neared the biochar surface, they displayed an increased charge density and a heightened affinity for the negatively charged sites. Pb (II) exchanges with the loosely bound cations [68].

$$Pb^{+2} + -COONa \rightarrow -COOPb + Na^+$$

$$Pb^{+2} + -COOK \rightarrow -COOPb + K^+$$

$$Pb^{+2} + -COOCa \rightarrow -COOPb + Ca^{+2}$$

$$Pb^{+2} + -COOMg \rightarrow -COOPb + Mg^{+2}$$

The O–H absorption at 3230 cm^{-1} for PTC 700 diminished post-adsorption, the C=O band at 1796 cm^{-1} and the COO^-/aromatic C=C peaked at 1566 cm^{-1} shifted, and the C–O peak at 1106 cm^{-1} exhibited reduced intensity, confirming surface complexation. Pb (II) ions established direct bonds with functional groups on the biochar surface, leading to the formation of stable spherical complexes. These ions are electrostatically associated with negatively charged functional groups, including carboxylate ($–COO^-$), hydroxyl (–OH), and alkoxide ($–O^-$) groups, while concurrently retaining their hydration shell of surrounding water molecules (H_2O) [69].

$$Pb^{+2} + \equiv COOH \rightarrow \equiv COOPb + H^+$$

$$Pb^{+2} + 2 \equiv COOH \rightarrow \equiv (COO)_2Pb + 2H^+$$

$$Pb^{+2} + \equiv OH \rightarrow \equiv OPb + H^+$$

New absorptions also appeared in the range below 600 cm^{-1}, further signifying the formation of Pb–O bonds. The FTIR results across all pyrolysis temperatures indicated that the primary active sites for Pb (II) adsorption via complexation, ion exchange, and surface precipitation consistently include hydroxyl, carbonyl, carboxyl, and phenolic groups. The minor discrepancies in peak positions and intensities indicate alterations in the structure and chemistry of biochar as the pyrolysis temperature increases.

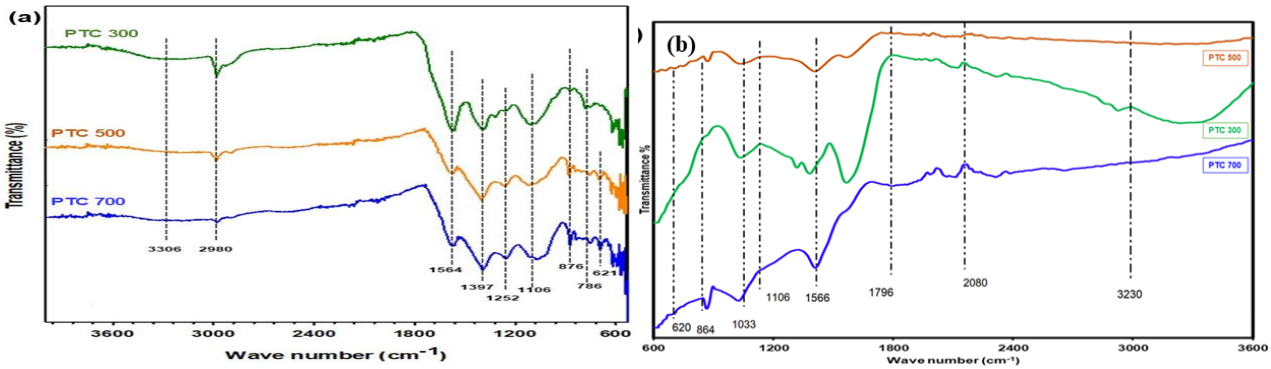

Figure 12. FTIR spectra of PTC 300, PTC 500 and PTC 700, respectively, (a) before adsorption of Pb (II), (b) after adsorption of Pb (II) from wastewater.

The SEM examination results (Figure 13) demonstrated that the biochar processed a highly porous structure, marked by a substantial presence of micropores, which enhanced its surface area and provided accessible pathways for the adsorption of Pb (II) ions. The complex pore structure facilitates the rapid passage of Pb (II) ions from the bulk solution into the internal framework of the biochar, leading to their physical trapping and immobilization [70]. Visual observations from SEM examination indicated an increase in pore abundance and accessibility, particularly for PTC 500, which correlated with enhanced Pb (II) adsorption capacity, despite the absence of quantitative measurements for specific surface area and pore size distribution in this study. Besides surface complexation and ion exchange mechanisms, the porous structure likely facilitated the diffusion of Pb (II) ions into internal adsorption sites, therefore occupying the pores. Consequently, pore filling may not be the sole determining factor, but rather an auxiliary process that enhances overall adsorption efficacy [71]. The micropores not only offer physical confinement but are also adorned with oxygen-containing functional groups. These groups enable further adsorption mechanisms, including cation exchange and surface complexation, thus

enhancing the overall uptake capacity. Ion exchange is proposed as a potential adsorption process owing to the presence of native cations and Pb (II) on the biochar surface.

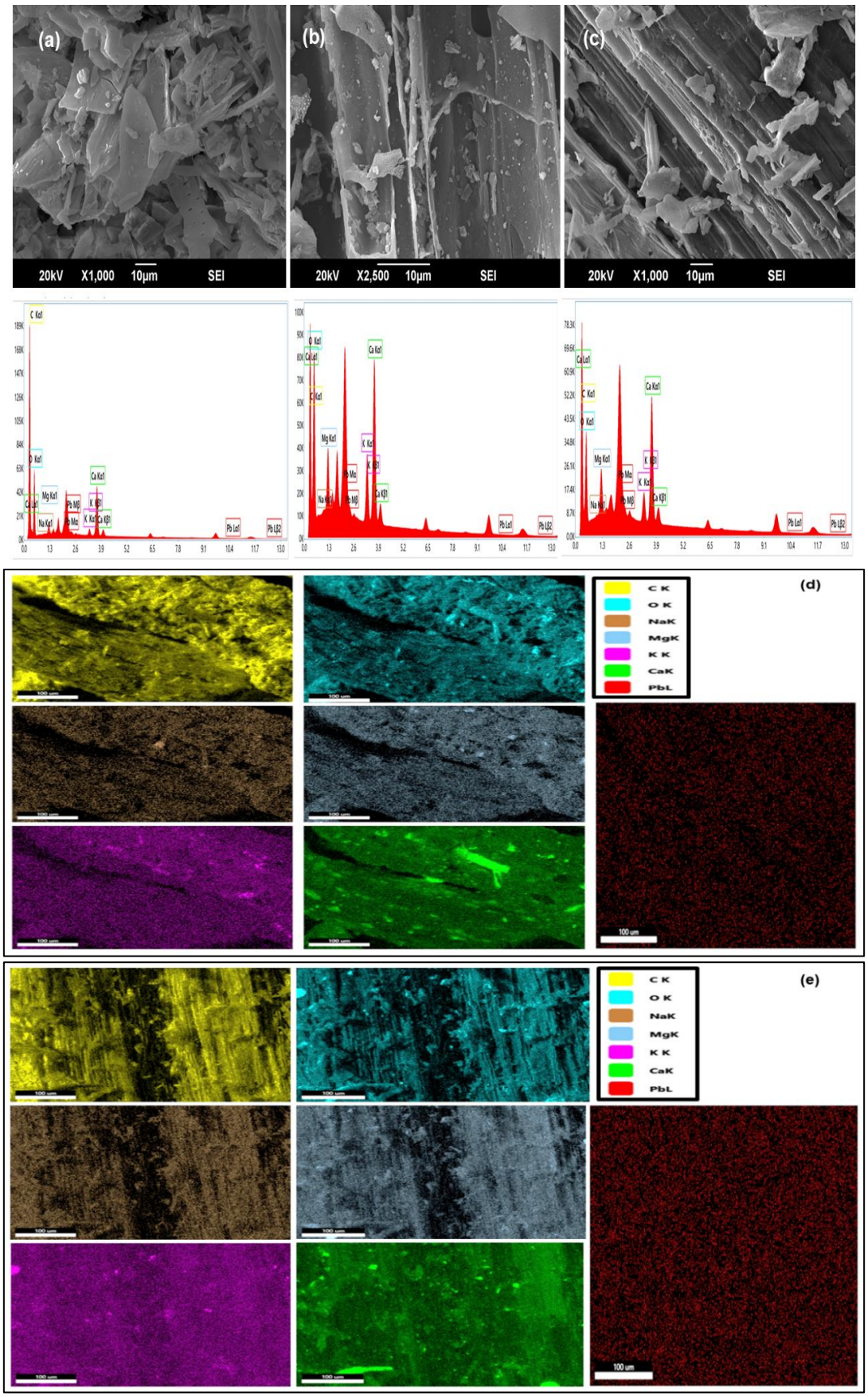

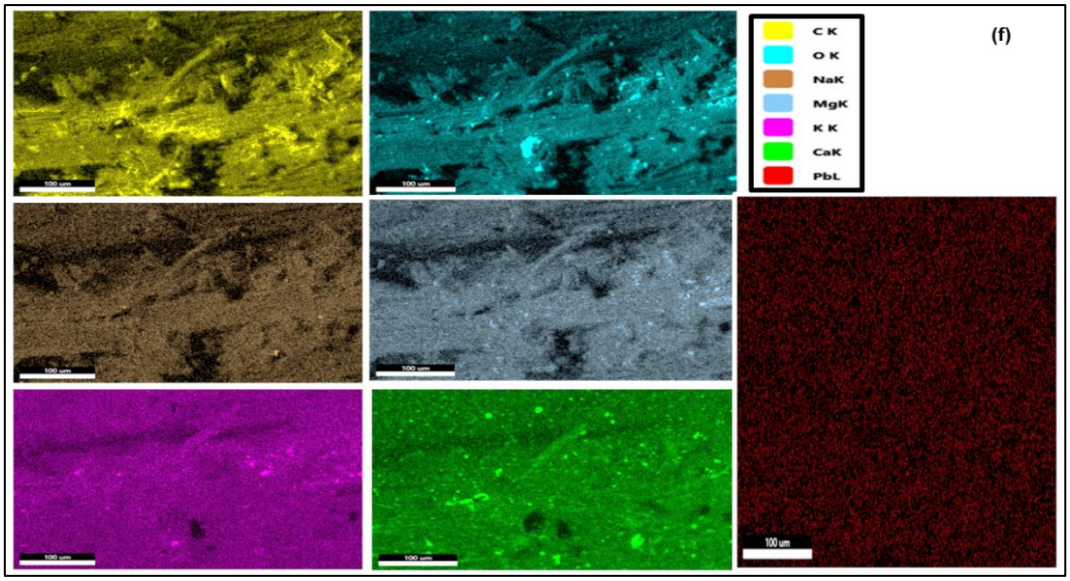

Figure 13. (a)–(c) SEM images with EDX spectra, (d)–(f) elemental mapping of PTC 300, PTC 500, and PTC 700, respectively, after adsorption of Pb (II).

Furthermore (Figure 14), the precipitation of Pb (II) species, including $Pb(OH)_2$ or $PbCO_3$, within the confined micropores contributes to the stabilisation of the adsorption process. The SEM results indicated that the porous and microporous structure of the biochar is crucial for the removal of Pb (II), facilitating a synergistic interaction among pore filling, ion exchange, and surface complexation mechanisms [72].

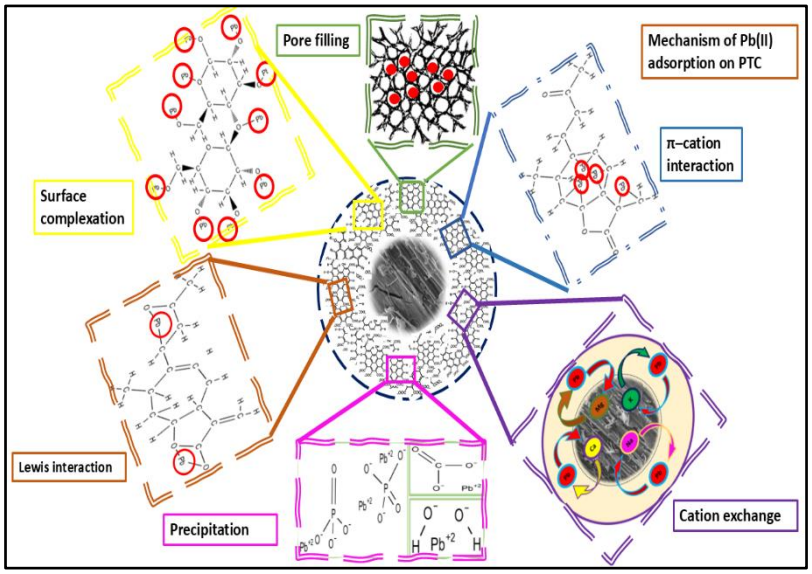

Figure 14. Overall mechanism of adsorption of Pb (II).

3.1.9. Future prospectives

The maximum Pb (II) adsorption capacity was recorded for PTC 500, owing to ion exchange with inherent mineral cations and surface complexation with oxygenated functional groups. In future studies,

researchers should focus on refining pyrolysis settings and post-activation techniques to enhance these active areas. Enhancing the immobilization and selectivity of Pb (II) can be achieved by altering the surface chemistry of biochar to increase the density of -COOH and -OH groups. Moreover, it is recommended to employ advanced spectroscopic techniques such as XPS to corroborate the proposed mechanisms and enhance comprehension of Pb binding states. To enhance the feasibility of employing biochar derived from parthenium for the continuous removal of Pb (II) from industrial wastewater, additional adjustment of fixed-bed operating parameters and extended regeneration studies are necessary. After reuse, PTCs functioned as a replacement for cement and aggregate in cementitious composites and were integrated into wood-polypropylene composites and plasters as an additive.

3.1.10. Proposed industrial mechanism

Figure 15 depicts a possible industrial layout for wastewater treatment. A continuous adsorptive water treatment method can be successfully illustrated by a rotating the arrangement of two parallel columns for wastewater treatment, as shown in the image. Examine two columns utilizing biochar as an adsorbent substance. Wastewater traverses Column A, whereby biochar efficiently eliminates lead and other pollutants. After the wastewater treatment is finalized, the flow is routed to Column B to maintain ongoing processing. Column B is purifying water, while Column A is subjected to a washing procedure using a specialized elution solvent to remove trapped contaminants, thus preparing Column A for reutilization. This cycle, in which A functions while B regenerates and then alternates, guarantees an uninterrupted process. The system's advantage is the concurrent processes of adsorption and regeneration, which eliminates the time and costs related to system downtime. It is more economical and minimizes supplementary pollutants.

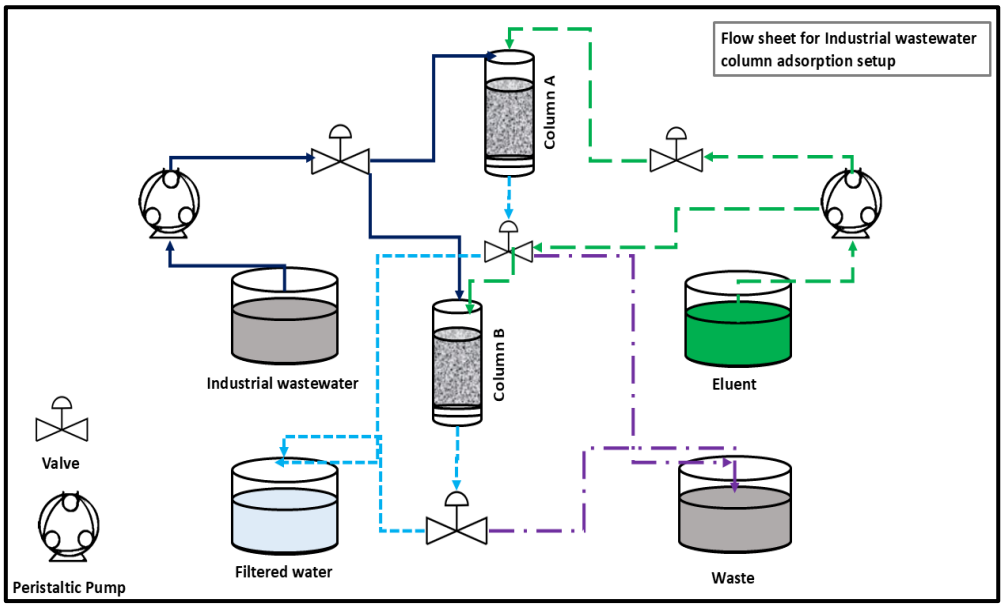

Figure 15. Proposed industrial configuration for wastewater treatment.

4. Conclusions

In this study, we evaluated a carbonaceous adsorbent derived from weeds, demonstrating effective adsorption of Pb (II). The thermal stability and adsorption capacity of PTCs were evaluated

by pyrolyzing them at 300, 500, and 700 ℃. Optimization of Pb (II) removal in batch studies was achieved at a concentration of 10 mg/L, pH 6, 1.5 g/L adsorbent and a contact duration of 45 minutes to attain adsorption equilibrium. PTC 500 surpassed PTC 300 and PTC 700, achieving 94% compared to 83% and 90%, respectively, owing to its superior pore structure and active sites at intermediate temperatures. The adsorption of PTC 500 was robust in batch and fixed-bed column methodologies. In addition to surface chemical groups, Lewis interactions, cation exchange, and π–π stacking interactions facilitated the removal of Pb (II). The batch adsorption experiment indicated that Pb (II) may interact with C-π in PTC 500. These procedures are proposed based on functional group analysis and relevant literature. Langmuir calculated a maximum adsorption capacity of 20.40 mg/g. The isotherm and kinetic data align closely with the Langmuir and pseudo-first-order theories. Adsorption evaluations on fixed-bed columns revealed the adsorbent's industrial viability. Lead (II) was removed from solutions containing various ions. The Clark model is most applicable when there is a higher initial Pb (II) concentration, reduced flow velocity, and increased bed height, all of which enhance Pb (II) sorption onto PTC. The greatest adsorption capacity in the fixed-bed column was 8.16 mg/g, indicating that varying conditions had a greater impact on external mass transfer at the outer layer. The Clark model, which most accurately aligned with the column data, confirmed the significance of film diffusion in breakthrough behavior. Consequently, film diffusion predominates in column operations, while pore diffusion governs batch adsorption, even when both resistances are involved. Producing saturated columns with 0.1 N CH_3COOH facilitates a minimum of five adsorption-desorption cycles. As such, PTC 500 has the potential to serve as an effective adsorbent for Pb (II) in the future.

Use of AI tools declaration

The authors declare they have not used Artificial Intelligence (AI) tools in the creation of this article.

Acknowledgments

The help, assistance, and support of the laboratory staff of Bahria University, Islamabad and Quaid-i-Azam University, Islamabad, are highly appreciated.

Kamran Younas: Writing–original draft, methodology, investigation, formal analysis, Asma Jamil: Writing–review & editing, supervision, Mahtab Ahmad: Writing–review & editing, co-supervision, providing lab facilities, Nazish Iftikhar: Writing–review & editing, validation, Qaisar Mahmood: Writing–review & editing, validation. Yung-Tse Hung: review & editing, validation.

Conflict of interest

Yung-Tse Hung and Qaisar Mahmood are the Guest Editors of special issue "Current advances in wastewater treatmet" for AIMS Environmental Science. Yung-Tse Hung and Qaisar Mahmood were not involved in the editorial review and the decision to publish this article.

References

1. Fernandez RMD, Estrada RJR, Tomon TRB, et al. (2023) Experimental design and breakthrough curve modeling of fixed-bed columns utilizing a novel 3D coconut-based Polyurethane-Activated carbon composite adsorbent for Lead sequestration. *Sustainability* 15. https://doi.org/10.3390/su151914344

2. Ahmed W, Mehmood S, Delgado AN, et al. (2021) Enhanced adsorption of aqueous Pb(II) by modified biochar produced through pyrolysis of watermelon seeds. *Sci Total Environ* 784: 147136. https://doi.org/10.1016/j.scitotenv.2021.147136
3. Zamfir FS, Carbureanu M, Mihalache SF (2025) Application of machine learning models in optimizing wastewater treatment processes: A review. *Appl Sci* 15. https://doi.org/10.3390/app15158360
4. Kumkum P, Kumar S (2024) A review on Biochar as an adsorbent for Pb (II) removal from water. *Biomass* 4: 243–272. https://doi.org/10.3390/biomass4020012
5. Baaloudj O, Langerame F, Iunnissi R, et al. (2025) Biochar-based downflow fixed-bed adsorption systems for water treatment: Process optimization, reusability, and techno-economic evaluation. *Sep Purif Technol* 377. https://doi.org/10.1016/j.seppur.2025.134347
6. Kumar S, Masto RE, Kaushik G (2023) Thermally processed biochar: Preparation, characterisation and their application for cadmium removal from surface and groundwater. *Int J Environ Anal Chem* 103: 6539–6558. https://doi.org/10.1080/03067319.2021.1958324
7. Jehan S, Khattak SA, Khan S, et al. (2023) Comparative efficacy of Parthenium hysterophorus (L.) derived biochar and iron doped zinc oxide nanoparticle on heavy metals (HMs) mobility and its uptake by Triticum aestivum (L.) in chromite mining contaminated soils. *Int J Phytoremediat* 25: 1890–1900. https://doi.org/10.1080/15226514.2023.2204968
8. Mondal S, Aikat K, Halder G (2016) Biosorptive uptake of ibuprofen by chemically modified Parthenium hysterophorus derived biochar: Equilibrium, kinetics, thermodynamics and modeling. *Ecol Eng* 92: 158–172. https://doi.org/10.1016/j.ecoleng.2016.03.022
9. Srivastava P, Raghubanshi AS (2021) I mpact of Parthenium hysterophorus L. invasion on soil nitrogen dynamics of grassland vegetation of Indo-Gangetic plains, India. *Environ Monit Assess* 193: 1–16. https://doi.org/10.1007/s10661-021-09070-6
10. Manjunath SV, Rakshitha D, Meghashree M, et al. (2024) Parthenium hysterophorus invasive weed valorization into biochar for removal of pharmaceuticals and personal care products: Competitive adsorption analysis via batch and fixed–bed column systems. *J Water Process Eng* 68. https://doi.org/10.1016/j.jwpe.2024.106578
11. Gwenzi W (2025) *Potential environmental and human health risks of biochar systems: A call for comprehensive health risk assessments*, In: Biochar for Environmental Remediation, Elsevier, 433–445.
12. Bashar HMK, Juraimi AS, Hamdani MSA, et al. (2021) A mystic weed, Parthenium hysterophorus: Threats, potentials and management. *Agronomy* 11: 1514. https://doi.org/10.3390/agronomy11081514
13. Ramola S, Rawat N, Shankhwar AK, et al. (2021) Fixed bed adsorption of Pb and Cu by iron modified bamboo, bagasse and tyre biochar. *Sustain Chem Pharm* 22. https://doi.org/10.1016/j.scp.2021.100486
14. Cheng P, Li ZK, Zheng YL, et al. (2025) Study on the regulation of performance and Hg0 removal mechanism of MIL-101(Fe)-derived carbon materials. *Sep Purif Technol* 379: 134939. https://doi.org/10.1016/j.seppur.2025.134939
15. Al-Saidi SS, Al-Haddabi M, Hassan SHA, et al. (2025) An investigation of using invasive weed (Parthenium hysterophorus) for sustainable boron removal from aqueous solutions. *Water Air Soil Poll* 237: 6. https://doi.org/10.1007/s11270-025-08623-6
16. Vallabha MS, Nagraj PC, Sanjeev NO, et al. (2025) Valorization of Parthenium hysterophorus weed into biochar for adsorptive removal of industrial dyes from multi-pollutant aqueous systems. *Biomass Convers Bior* 15: 24227–24241.https://doi.org/10.1007/s13399-024-05534-0

17. APHA (2017) *Standard methods for the examination of water and wastewater*, American Public Health Association.
18. Qurat ul A, Shafiq M, Capareda SC, et al. (2021) Effect of different temperatures on the properties of pyrolysis products of Parthenium hysterophorus. *J Saudi Chem Soc* 25: 101197–101197. https://doi.org/10.1016/j.jscs.2021.101197
19. Islam Iu, Ahmad M, Shah B, et al. (2024) Parthenium hysterophorus-derived iron-coated biochar: a sustainable solution for nitrate and phosphate removal from water. *Biomass Convers Bior* 15: 10773–10790. https://doi.org/10.1007/s13399-024-05821-w
20. Ebeid H, Di Gianvincenzo F, Cigić IK, et al. (2024) Chromatographic analysis of natural dyes in mediaeval Islamic paper. *Herit Sci* 12: 13. https://doi.org/10.1186/s40494-023-01117-w
21. Mondal S, Aikat K, Siddharth K, et al. (2017) Optimizing ranitidine hydrochloride uptake of Parthenium hysterophorus derived N-biochar through response surface methodology and artificial neural network. *Process Saf Environ* 107: 388–401. https://doi.org/10.1016/j.psep.2017.03.011
22. Hasan M, Al Biruni MT, Azad S, et al. (2024) Adsorptive removal of dye from textile wastewater employing Moringa oleifera leaves biochar as a natural biosorbent. *Biomass Convers* 14: 11075–11091. https://doi.org/10.1007/s13399-022-03196-4
23. Kanagalakshmi M, Devi SG, Ananthi P, et al. (2024) *Adsorption isotherms and kinetic models*, In: Tharini J, Thomas S, Eds., Carbon Nanomaterials and their Composites as Adsorbents, Cham: Springer International Publishing, 135–154.
24. González-Fernández LA, Aguirre-Contreras S, Medellín-Castillo NA, et al. (2025) Mathematical modelling of kinetic and breakthrough curves for Cd (II) adsorption onto Sargassum biomass using the diffusion–permeation model. *J Water Process Eng* 77: 108473. https://doi.org/10.1016/j.jwpe.2025.108473
25. Al-Mahbashi NMY, Kutty SRM, Bilad MR, et al. (2022) Bench-scale fixed-bed column study for the removal of dye-contaminated effluent using sewage-sludge-based biochar. *Sustainability* 14: 6484. https://doi.org/10.3390/su14116484
26. Sadaf S, Bhatti HN (2014) Batch and fixed bed column studies for the removal of Indosol Yellow BG dye by peanut husk. *J Taiwan Inst Chem E* 45: 541–553. https://doi.org/10.1016/j.jtice.2013.05.004
27. Georgieva V, Gonsalvesh L, Mileva S, et al. (2025) Evaluation of heavy metal adsorption efficiency of biochars derived from agricultural waste. *Biomass* 5. https://doi.org/10.3390/biomass5020033
28. Sopanrao KS, Sreedhar I (2025) Novel coal fly ash–chitosan composite for highly efficient, cost-effective and stable removal of lead and chromium from industrial wastewater. *Environ Sci-Wat Res* 11: 1977–2001. https://doi.org/10.1039/d5ew00257e
29. Maneechakr P, Karnjanakom S (2019) Environmental surface chemistries and adsorption behaviors of metal cations (Fe(3+), Fe(2+), Ca(2+) and Zn(2+)) on manganese dioxide-modified green biochar. *RSC Adv* 9: 24074–24086. https://doi.org/10.1039/c9ra03112j
30. Choudhary V, Patel M, Pittman CU Jr, et al. (2020) Batch and continuous fixed-bed Lead removal using Himalayan Pine Needle biochar: Isotherm and kinetic studies. *ACS Omega* 5: 16366–16378. https://doi.org/10.1021/acsomega.0c00216
31. Tejada-Tovar C, Villabona-Ortíz Á, Gonzalez-Delgado Á, et al. (2025) Simulation of Pb(II) and Ni(II) adsorption in a Packed Column: Effects of bed height, flow rate, and initial concentration on performance metrics. *Processes* 13. https://doi.org/10.3390/pr13072141

32. Subramanian P, Pakkiyam S, Pandian K, et al. (2024) Preparation and modification of Prosopis juliflora biochar and Pb (II) removal from aqueous solutions. *Biomass Convers Bior* 15: 421–435. https://doi.org/10.1007/s13399-024-05575-5
33. Mustapha LS, Yusuff AS, Dim PE (2023) Heliyon RSM optimization studies for cadmium ions adsorption onto pristine and acid-modified kaolinite clay. *Heliyon* 9: e18634–e18634. https://doi.org/10.1016/j.heliyon.2023.e18634
34. Atugoda T, Gunawardane C, Ahmad M, et al. (2021) Mechanistic interaction of ciprofloxacin on zeolite modified seaweed (Sargassum crassifolium) derived biochar: Kinetics, isotherm and thermodynamics. *Chemosphere* 281: 130676–130676. https://doi.org/10.1016/j.chemosphere.2021.130676
35. Fan J, Shi J, Zhao Y, et al. (2025) Interaction between nano-biochar and Pb during migration in saturated porous media: Impact of ionic strength, pH and flow velocity. *Colloid Surfac A* 717: 136720. https://doi.org/10.1016/j.colsurfa.2025.136720
36. Gao Z, Shan D, He J, et al. (2023) Effects and mechanism on cadmium adsorption removal by CaCl2-modified biochar from selenium-rich straw. *Bioresource Technol* 370: 128563–128563. https://doi.org/10.1016/j.biortech.2022.128563
37. Ramola S, Belwal T, Srivastava RK (2020) Thermochemical conversion of biomass waste-based biochar for environment remediation. *Handbook Nanomater Nanocomposit Energy Environ Appl* 1–16. https://doi.org/10.1007/978-3-030-11155-7_122-2
38. Annane K, Lemlikchi W, Tingry S (2023) Efficiency of eggshell as a low-cost adsorbent for removal of cadmium : kinetic and isotherm studies. *Biomass Convers Bior* 6163–6174. https://doi.org/10.1007/s13399-021-01619-2
39. Akhtar L, Ahmad M, Iqbal S, et al. (2021) Biochars' adsorption performance towards moxifloxacin and ofloxacin in aqueous solution: Role of pyrolysis temperature and biomass type. *Environ Technol Inno* 24: 101912–101912. https://doi.org/10.1016/j.eti.2021.101912
40. Ravindiran G, Sundaram H, Rajendran EM, et al. (2023) Removal of azo dyes from synthetic wastewater using biochar derived from sewage sludge to prevent groundwater contamination. *Urban Clim* 49: 101502. https://doi.org/10.1016/j.uclim.2023.101502
41. Khalid U, Inam MA (2024) The influence of pyrolysis temperature on the performance of cotton stalk biochar for Hexavalent Chromium removal from wastewater. *Water Air Soil Poll* 235. https://doi.org/10.1007/s11270-024-06922-y
42. Banerjee P, Hazra A, Ghosh P, et al. (2019) *Waste management and resource efficiency*, Singapore: Springer.
43. Mahmoud ME, Abdelfattah AM, Tharwat RM, et al. (2020) Adsorption of negatively charged food tartrazine and sunset yellow dyes onto positively charged triethylenetetramine biochar: Optimization, kinetics and thermodynamic study. *J Mol Liq* 318: 114297. https://doi.org/10.1016/j.molliq.2020.114297
44. Chung NT, Thuy DT, Trang LH, et al. (2025) Evaluating coffee husk biochar as a sustainable and novel adsorbent for lead and copper in wastewater. *Biomass Convers Bior* 15: 18437–18453. https://doi.org/10.1007/s13399-025-06674-7
45. Su Y, Liao Q, Xia S, et al. (2025) Adsorption of heavy metal Pb(II) in dredged sediment using different biochar materials. *Processes* 13. https://doi.org/10.3390/pr13040957
46. Younas K, Jamil A, Saleem ARJEQM (2023) Carcinogenic effect of potential toxic metals in school children through contaminated drinking water around the industrial area of Pakistan. *Environ Qual Manag* 32: 19–30. https://doi.org/10.1002/tqem.21979

47. Khamkure S, Treesatayapun C, Terrones VB, et al. (2026) A fuzzy-driven synthesis: MiFREN-optimized magnetic biochar nanocomposite from agricultural waste for sustainable Arsenic water remediation. *Technologies* 14: 43. https://doi.org/10.3390/technologies14010043
48. Liu N, Zhou R, Huang S, et al. (2025) Effects of ferrite porous confined biochar nanoreactor on the adsorption and desorption of Pb and Cd. *J Water Process Eng* 74: 107717. https://doi.org/10.1016/j.jwpe.2025.107717
49. Wu J, Sun X, Wu J, et al. (2025) Eggshell-enhanced biochar with in-situ formed $CaO/Ca(OH)_2$ for efficient removal of Pb^{2+} and Cd^{2+} from wastewater: Performance and mechanistic insights. *Sep Purif Technol* 354: 129352. https://doi.org/10.1016/j.seppur.2024.129352
50. Irfan I, Inam MA, Usmani W, et al. (2023) Adsorptive recovery of phosphate using iron functionalized biochar prepared via co-pyrolysis of wheat straw and sewage sludge. *Environ Technol Inno* 32. https://doi.org/10.1016/j.eti.2023.103434
51. Omara P, Singh H, Singh K, et al. (2023) Short-term effect of field application of biochar on cation exchange capacity, pH, and electrical conductivity of sandy and clay loam temperate soils. *Technol Agronomy* 3: 16. https://doi.org/10.48130/TIA-2023-0016
52. Mesfer MKA, Danish M, Khan MI, et al. (2020) Continuous fixed bed CO_2 adsorption: breakthrough, column efficiency, mass transfer zone. *Processes* 8: 1233. https://doi.org/10.3390/pr8101233
53. Almeida ENd, Pacheco EA, Nagahama KJ, et al. (2024) Adsorption kinetics of tartrazine dye on activated carbon derived from Guava (Psidium guajava) seeds. *J Brazil Chem Soc* 35: e-20240139. https://doi.org/10.21577/0103-5053.20240139
54. Yan J, Xue Y, Long L, et al. (2018) Adsorptive removal of As(V) by crawfish shell biochar: batch and column tests. *Environ Sci Pollut R* 25: 34674–34683. https://doi.org/10.1007/s11356-018-3384-1
55. Shakeel A, Khan IM, Jeelani F, et al. (2025) Comparative chromium adsorptive capacity of different low-cost materials using fixed bed column. *Sci Rep* 15: 26876. https://doi.org/10.1038/s41598-025-12076-6
56. Rathi TA, Gomase V, Saravanan D, et al. (2024) Mathematical modelling for fixed-bed column and batch adsorption studies of antibiotic and CO_2 capture using soybean stover biochar. *BioNanoScience* 15. https://doi.org/10.1007/s12668-024-01694-5
57. Hussain F, Kim LH, Oh SE, et al. (2025) Neutralization of pH and removal of heavy metals from acid mine water by using low-cost biosorbents in batch and column studies. *Groundwater Sustain Develop* 31. https://doi.org/10.1016/j.gsd.2025.101506
58. El-Sayed NS, Kamal KH, El-Sakhawy M, et al. (2025) High-efficiency removal of lead (II) and methylene blue by MnO_2-decorated oxidized biochar. *J Water Process Eng* 72. https://doi.org/10.1016/j.jwpe.2025.107478
59. Suter E, Rutto H, Omwoyo W (2025) Continuous packed bed column removal of Cr^{6+}, Cd^{2+}, and Pb^{2+} ions from synthetic wastewater using polymeric ultra-permeable and biodegradable ferromagnetic nanocomposite membrane. *Can J Chem Eng* 103: 2642–2658. https://doi.org/10.1002/cjce.25555
60. Bakhta S, Sadaoui Z, Bouazizi N, et al. (2024) Successful removal of fluoride from aqueous environment using $Al(OH)_3$@AC: Column studies and breakthrough curve modeling. *RSC Adv* 14: 1–14. https://doi.org/10.1039/D3RA06697E
61. Mani SK, Bhandari R (2022) Efficient fluoride removal by a fixed-bed column of self-assembled Zr(IV)-, Fe(III)-, Cu(II)-complexed polyvinyl alcohol hydrogel beads. *ACS Omega* 7: 15048–15063. https://doi.org/10.1021/acsomega.2c00834

62. Ali MA, Mubarak MF, Keshawy M, et al. (2022) Adsorption of Tartrazine anionic dye by novel fixed bed Core-Shell-Polystyrene Divinylbenzene/Magnetite nanocomposite. *Alex Eng J* 61: 1335–1352. https://doi.org/10.1016/j.aej.2021.06.016
63. Fito J, Abewaa M, Nkambule T (2023) Magnetite-impregnated biochar of parthenium hysterophorus for adsorption of Cr (VI) from tannery industrial wastewater. *Appl Water Sci* 13: 1–23. https://doi.org/10.1007/s13201-023-01880-y
64. Zhao R, Li X, Jiang X, et al. (2026) Pyrolysis temperature dependence of Pb^{2+} removal by sewage sludge biochar: characteristic evaluation and adsorption performance. *Environ Sci Adv* 5: 900–916. https://doi.org/10.1039/D5VA00202H
65. Zhang Y, Zhang L, Han C, et al. (2023) Preparation, characteristics and mechanisms of Cd(II) adsorption from aqueous solution by mango kernel-derived biochar. *Biomass Convers Bior* 13: 393–407. https://doi.org/10.1007/s13399-022-03050-7
66. Lee JI, Jo JS, Lee YJ, et al. (2025) Mechanistic insights and process optimization of perilla frutescens stem biochar for cadmium removal from zinc smelter wastewater. *Appl Water Sci* 16: 2. https://doi.org/10.1007/s13201-025-02673-1
67. Meshram S, Dharmadhikari S, Thakur RS, et al. (2023) Fixed-bed adsorption of lead from battery recycling unit wastewater-optimization using Box-Behnken method. *J Hazard Mater Adv* 10. https://doi.org/10.1016/j.hazadv.2023.100297
68. Chistie SM, Naik SU, Rajendra P, et al. (2025) Production and characterization of magnetic Biochar derived from pyrolysis of waste areca nut husk for removal of methylene blue dye from wastewater. *Sci Rep* 15: 23209. https://doi.org/10.1038/s41598-025-03359-z
69. Souza TF, Fernandes LF, Batista LMdS, et al. (2026) Fe–Mn biochar composites from sugarcane bagasse for Herbicides removal: Structure, mechanisms, and safety relationships toward sustainable water treatment. *ACS Omega* 11: 8704–8721. https://doi.org/10.1021/acsomega.5c12317
70. Charboub F, Ait Akbour R, Laabd M, et al. (2026) Eucalyptus camaldulensis leaves-derived biochar for effective removal of Cd(II) and Pb(II) ions from aqueous solutions. *Int J Phytoremediat* 28: 105–114. https://doi.org/10.1080/15226514.2025.2552497
71. Zhang M, Liu G, Liu R, et al. (2025) Efficient flocculation of multiple heavy metals by iron-based modified-carbonate biochar: Adsorption mechanism and practical application. *J Environ Chem Eng* 13: 115120. https://doi.org/10.1016/j.jece.2024.115120
72. Wang Y, Liu Y, Chao T, et al. (2026) High efficiency adsorption of Cd(II) by $KHCO_3$-activated Fe/Mn co-modified peanut shell biochar: Adsorption performance, mechanisms, and life cycle assessment. *Chem Eng Sci* 321. https://doi.org/10.1016/j.ces.2025.122747